



UPPSALA  
UNIVERSITET

*Digital Comprehensive Summaries of Uppsala Dissertations  
from the Faculty of Science and Technology 774*

# Analytical Aerodynamic Simulation Tools for Vertical Axis Wind Turbines

PAUL DEGLAIRE



ACTA  
UNIVERSITATIS  
UPSALIENSIS  
UPPSALA  
2010

ISSN 1651-6214  
ISBN 978-91-554-7913-8  
urn:nbn:se:uu:diva-132073

Dissertation presented at Uppsala University to be publicly examined in Högskolan, Ångström Laboratory, Lagerhyddsvägen 1, Uppsala, Friday, November 26, 2010 at 10:00 for the degree of Doctor of Philosophy. The examination will be conducted in English.

### **Abstract**

Deglaire, P. 2010. Analytical Aerodynamic Simulation Tools for Vertical Axis Wind Turbines. Acta Universitatis Upsaliensis. *Digital Comprehensive Summaries of Uppsala Dissertations from the Faculty of Science and Technology* 774. 100 pp. Uppsala. ISBN 978-91-554-7913-8.

Wind power is a renewable energy source that is today the fastest growing solution to reduce CO<sub>2</sub> emissions in the electric energy mix. Upwind horizontal axis wind turbine with three blades has been the preferred technical choice for more than two decades. This horizontal axis concept is today widely leading the market. The current PhD thesis will cover an alternative type of wind turbine with straight blades and rotating along the vertical axis. A brief overview of the main differences between the horizontal and vertical axis concept has been made. However the main focus of this thesis is the aerodynamics of the wind turbine blades.

Making aerodynamically efficient turbines starts with efficient blades. Making efficient blades requires a good understanding of the physical phenomena and effective simulations tools to model them. The specific aerodynamics for straight bladed vertical axis turbine flow are reviewed together with the standard aerodynamic simulations tools that have been used in the past by blade and rotor designer. A reasonably fast (regarding computer power) and accurate (regarding comparison with experimental results) simulation method was still lacking in the field prior to the current work. This thesis aims at designing such a method.

Analytical methods can be used to model complex flow if the geometry is simple. Therefore, a conformal mapping method is derived to transform any set of section into a set of standard circles. Then analytical procedures are generalized to simulate moving multibody sections in the complex vertical flows and forces experienced by the blades. Finally the fast semi analytical aerodynamic algorithm boosted by fast multipole methods to handle high number of vortices is coupled with a simple structural model of the rotor to investigate potential aeroelastic instabilities.

Together with these advanced simulation tools, a standard double multiple streamtube model has been developed and used to design several straight bladed rotor ranging from 2 kW to 20 kW.

*Keywords:* vertical axis turbine, vortex flows, conformal mapping, analytical aerodynamics, potential flows, fast multipole methods

*Paul Deglaire, Department of Engineering Sciences, Electricity, Box 534, Uppsala University, SE-75121 Uppsala, Sweden.*

© Paul Deglaire 2010

ISSN 1651-6214

ISBN 978-91-554-7913-8

urn:nbn:se:uu:diva-132073 (<http://urn.kb.se/resolve?urn=urn:nbn:se:uu:diva-132073>)

*To MLPS, my parents  
and my grand parents*



# List of Papers

This thesis is based on the following papers, which are referred to in the text by their Roman numerals.

- I **P. Deglaire**, O. Ågren, H. Bernhoff, M. Leijon. Conformal mapping and efficient boundary element method without boundary elements for fast vortex particle simulations. *European Journal of Mechanics – B Fluids*, Volume 27, Issue 2, March-April 2008, Pages 150-176.
- II **P. Deglaire**, S. Engblom, O. Ågren, H. Bernhoff. Analytical solutions for a single blade in vertical axis turbine motion in two-dimensions, *European Journal of Mechanics – B Fluids*, Volume 28, Issue 4, July-August 2009, Pages 506-520.
- III D Österberg, **P. Deglaire**, H. Bernhoff, M. Leijon, A Multi-Body Vortex Method Applied to Vertical Axis Wind Turbines. Submitted to the *European Journal of Mechanics – B Fluids* in Nov 2010.
- IV M. Bouquerel, **P. Deglaire**, H. Bernhoff, M. Leijon, Fast aeroelastic model for straight bladed vertical axis wind and hydro turbines submitted to the *Wind Engineering Journal* in July 2010.
- V K. Yuen, K. Thomas, M. Grabbe, **P. Deglaire**, M. Bouquerel, D. Österberg, M. Leijon. Matching a permanent magnet synchronous generator to a fixed pitch vertical axis turbine for marine current energy conversion. *IEEE Journal of Ocean Engineering*, vol 34, no1, pp24-31, Jan 2009.
- VI A. Solum, **P. Deglaire**, S. Eriksson, M. Stålberg, M. Leijon and H. Bernhoff. Design of a 12kW vertical axis wind turbine equipped with a direct driven PM synchronous generator. EWEC 2006 - European Wind Energy Conference & Exhibition, Athens, Greece
- VII **P. Deglaire**, S. Eriksson, J. Kjellin and H. Bernhoff. Experimental results from a 12 kW vertical axis wind turbine with a direct driven PM synchronous generator. EWEC 2007 - European Wind Energy Conference & Exhibition, Milan, Italy.
- VIII J. Kjellin, S. Eriksson, **P. Deglaire**, F. Bülow and H. Bernhoff. Progress of control system and measurement techniques for a 12 kW vertical axis wind turbine. *Scientific proceedings of EWEC 2008 - European Wind Energy Conference & Exhibition*:186-190.

Reprints were made with permission from respective publishers.



# Contents

1. Introduction.....	13
1.1 Aim of the thesis .....	14
1.2 Outline of the thesis.....	15
1.3 The concept .....	16
2. Background.....	19
2.1 Historical overview of wind power and VAWTs.....	19
2.2 Working principle of VAWTs.....	23
2.2 Aerodynamic efficiency measures .....	26
2.3 Current VAWT projects .....	27
2.4 Aerodynamic specificities of H-rotor flows .....	30
2.5 Benefit and drawbacks of aerodynamic approaches .....	32
3. Semi analytical theory of unsteady aerodynamics .....	35
3.1 Equations.....	35
3.1.1. Mass conservation .....	36
3.1.2. Navier Stokes equations .....	41
3.1.3. Vorticity and vorticity transport .....	41
3.1.4. Bernoulli equations.....	45
3.1.5. Strategy of solution for the multibody problems .....	46
3.2 Geometry– boundary conditions .....	47
3.3 Conformal mapping.....	50
3.4 Analytical solutions.....	52
3.4.1. Solution of the single blade problem with vortices .....	52
3.4.2. Velocity field .....	53
3.4.3. Kutta condition .....	53
3.4.4. Numerical implementation .....	54
3.4.5. Forces evaluation.....	54
3.4.6. Synthesis of the single blade analytical solution .....	55
3.4.7. Multiblade solution.....	56
3.5 Aeroelasticity .....	57
3.6 Lower order models .....	58
4 Design studies .....	62
4.1 Comparison with benchmark cases .....	62
4.1.1. Conformal mapping test case.....	62
4.1.2. Unsteady single blade test case.....	63

4.2 VAWT measurement comparisons .....	66
4.2.1. Unsteady Normal and tangential forces .....	66
4.2.2. Cp curve comparisons .....	70
4.2.3. Wake studies .....	72
4.2.4. Aeroelastic analysis .....	74
4.3 New design studies .....	75
4.3.1 Marsta turbine .....	78
4.3.2 A turbine for the South Pole Amundsen station .....	79
4.3.3 Other wind and underwater design studies .....	80
4.3.4 Aeroelastic studies .....	81
4.4 Perspectives of the model .....	84
Suggestions for future work .....	88
Summary of papers .....	89
Conclusion .....	92
Acknowledgments .....	93
Summary in Swedish .....	94
References .....	97



# Nomenclature and abbreviations

For all the following otherwise mentioned, all geometrical parameters are given in the turbine horizontal plane

Symbol	Unit	Real or complex number	Explanation
$a$	m	Real	Instantaneous distance between the turbine center and the section. If constant: radius of turbine for an H-rotor
$A$	$m^2$	Real	Wind turbine frontal area or swept area
$A_p$	$m^2$	Real	Profile area
AR Aspect Ratio	Non dimensional	Real	Ratio of the blade height by the blade chord. In non constant chord blades it is the ratio of the square of the wingspan divided by the area of the wing planform.
$b$	m	Real	Radius of the circle representing the airfoil section.
$c$	m	Real	Blade chord
$\{c_k\}_{k \in \mathbb{N}}$	NA	Complex	Coefficient of the Laurent serie decomposition of $f$ .
$C_N$	Non dimensional	Real	Normal force coefficient acting on a blade section.
$C_P$	Non dimensional	Real	Aerodynamic efficiency factor.
$C_{Pr}$	Non dimensional	Real	Pressure coefficient
$C_T$	None	Real	Tangential force coefficient acting on a blade section.
curl()	Unit/m	Complex	Operator. Curl
$d/dt$	Unit/s	NA	Operator. Lagrangian derivative
div()	Unit/m	Real	Operator. Divergence
$e$	NA	Complex	Complex exponential function
$f$	NA	Complex	Complex function of complex arguments. Conformal transformation in the case of single section transform
$F$	$m^2/s$	Complex	Complex function of complex numbers. Complex potential
$f_r$	Hz	Real	Pitching, heaving or plunging frequency

$\{G_k\}_{k \geq 1}$	NA	Complex	Coefficient of the Laurent's serie of the complex potential solution of the irrotational, inviscid incompressible single blade H-rotor flow
$g$	NA	Complex	Complex function of complex arguments. Conformal transformation in the case of multiple section transform
$i$	Non dimensional	Complex	Pure imaginary number such that $i^2 = -1$
$\text{Im}()$	Non dimensional	Real	Operator. Imaginary part of a complex number
$k$	Hz	Real	Reduced frequency for unsteady aerodynamics analysis
$M_0$	N.m	Real	Pitching moment of the section
$N$	Non dimensional	Real	Number of coefficient used in the Laurent series expansion of $f$
$N_W$	Non dimensional	Real	Real number/ Number of blades or wings for an H-rotor
$N_f$	N	Real	Normal force acting on a blade section per height unit
$p$	Pa	Real	Real function of complex number. Pressure field
$P_m$	W	Real	Mechanical power output neglecting all losses in bearings, gearboxes and electrical circuit
$p_\infty$	Pa	Real	Pressure at infinity upwind
$r_C$	m	Real	Radius of vortex kernel
$\text{Re}()$	Non dimensional	Real	Operator. Real part of a complex number
$R_e$	Non dimensional	Real	Reynolds number: measure of the inertia effect versus the viscous effects in a fluid.
$s = x + iy$	m	Complex	Generic complex number of real part $x$ and imaginary part $y$
$s_C$	m	Complex	Points in the circle which are the reverse image of the airfoil points through $f$
$s_{ol}$	Non dimensional	Real	H-rotor solidity
$S_V$	m	Complex	Position of vortex kernel center
$t$	s	Real	Time measure
$T_{an}$	m	Complex	Tangent vector along the blade
$T_f$	N	Complex	Tangential force acting on a blade section per height unit
$\underline{U} = U_x + iU_y$	m/s	Complex	Complex number but function of real numbers. Velocity field in Eulerian coordinates

---

$V$	m/s	Complex	Complex function of complex numbers. Velocity field in Eulerian coordinates
$V_0$	m/s	Real	Instantaneous asymptotic incoming wind speed
$V_{z/z_3inz}$	m/s	Complex	Complex function. Velocity of a point attached to the $z$ frame expressed in the $z_3$ frame
$V_\theta$	m/s	Real	Tangential velocity
$W_{seen}$	m/s	Complex	Relative wind seen by the blade section
$X, Y$	N	Real	Real numbers. Real and imaginary part of the forces seen by the section.
$x_0$	m	Real	Blade shift position
$z$	m	Complex	Position of points in the frame attached to the section
$z_3$	m	Complex	Position of points in the earth frame.
$z_{blade}$	m	Complex	Blade position
$z_{Ci} = x_{Ci} + iy'_{Ci}$	m	Complex	Position of points in the airfoil section
$\alpha$	rad	Real	Instantaneous angle of the incoming wind speed with respect to the wind speed reference.
$\beta$	rad	Real	Real number Instantaneous angular position of the blade
$\Gamma_V$	m <sup>2</sup> /s	Real	Vortex kernel circulation
$\delta$	rad	Real	Pitch angle of blades
$\Delta$	Unit/m <sup>2</sup>	NA	Laplacian operator
$\nabla$	Unit/m	NA	Nabla differential operator
$\eta_{TE}$	rad	Real	Trailing edge angle in the transformed circle plane
$\vartheta$	rad	Real	Local angle of attack of the wind speed seen by the blade
$\lambda$ or TSR	Non dimensional	Real	H-rotor tip speed ratio
$\rho$	kg.m <sup>-3</sup>	Real	Fluid mass density
$\sigma_0$	m	Real	Constant in the conformal transformation
$\varphi$	m <sup>2</sup> /s	Real	Real function of complex number. Potential function
$\psi$	m <sup>2</sup> /s	Real	Real function of complex number. Streamfunction
$\omega$	/s	Real	Real function of complex numbers. Vorticity field for two dimensional flows
$\underline{\omega}$	/s	Real	Three dimensional vector. Vorticity field.
$\omega_f$	rad/s	Real	Pulsation corresponding to $f_r$
$\omega_R$	rad/s	Real	Instantaneous turbine rotational speed.

---

---

BEM	NA	Blade Element Momentum theory
CFD	NA	Computational Fluid Dynamics
CMDMS	NA	Name of the multiple streamtube code developed. Stands for Conformal Mapping Double Multiple Streamtube.
DNS	NA	Direct Numerical simulation to solve Navier Stokes equations
DMST	NA	Double Multiple Streamtube model
ElasTechs	NA	Name of the elastic model for strut and blades developed
FEM	NA	Finite Element Method
FFM	NA	Fast Multipole Method
FVM	NA	Finite Volume Method
HAWT	NA	Horizontal Axis Wind Turbine
LES	NA	Large Eddy Simulation
PDE	NA	Partial Differential Equation
SNL	NA	Sandia National Laboratories
VAWT	NA	Vertical Axis Wind Turbine
VoreTechs	NA	Name of the free wake vortex model developed here
VoreElasTechs	NA	Name of the couple code VoreTechs and ElasTechs

---

# 1. Introduction

A sustainable future with limited atmospheric CO<sub>2</sub> emissions and growing energy needs forces us to consider alternative energy sources to oil, gas and coal.

The situation is more than worrying as the impact on the earth climate will be incurable without a swift move to clean energy.

Temperature increase	CO <sub>2</sub> emissions 2050 (compared with % of 2000 emissions)
2.0 – 2.4	-85 to -50
2.4 – 2.8	- 60 to -30
2.8 – 3.2	-30 to +5
3.2 - 4	+10 to +60

Table 1. Temperature increase in 2050 compared with 2000 level depending on the level of CO<sub>2</sub> emission according to [1]

In 2007, the electrical power generation accounted for 29% [2] of the atmospheric CO<sub>2</sub> emissions. Reducing this source will not solve the problem but can significantly contribute to its solution.

None of the CO<sub>2</sub> free technologies that are technically mature today, or in the near future can on its own, tackle the problem. A global solution must also provide capacity to match the fluctuating demand. Therefore storage and transmission networks are also key factors.

Wind power is a strong candidate towards a sustainable future: wind power with hydro power, are among the most cost effective renewables. For many countries, with its relatively fast development potential, wind power represents a good starting point for developing renewable energy sources, although, due to its variability, it cannot aim to be the sole electricity source for a single country.

Wind power has been commercially successful in Europe for more than a decade. European countries have more than 70 GW installed capacity with 5 top leading countries: Germany with 25,777 MW, Spain 18,320 MW, Italy 4,850 MW, France 4,492 MW and UK 4,070 MW [3]. Although Europe has been the number one region when it comes to new yearly installed capacity

for more than a decade, US and China are now moving ahead. In Europe offshore wind power opens a new arena for wind developments, especially in the North Sea.

The world's leading manufacturers were originally situated in countries where local incentives have accelerated the installation of turbines namely Germany, Denmark and Spain. Now fast emerging markets like US, China and India have pushed strong local suppliers. The market leaders are today Vestas (Denmark) 12.5%, GE Energy (US) 12.4%, Sinovel (China) 9.2%; Enercon (Germany) 8.5%, Goldwind (China) 7.2% and Gamesa (Spain) 6.7% [4].

The total market in 2009 represents around 30 GW for wind turbine manufacturers leading to a total turnover of 30 billions Euros.

In terms of technology, the market is dominated by three bladed upwind horizontal axis wind turbines (HAWTs) with gearbox and asynchronous generators.

The current thesis will concern a less well known but emerging technology, the vertical axis wind turbines (VAWTs). In particular this thesis will be focused on a special type of VAWT with straight blades also referred to as an H rotor, the H representing its cross vertical section.

## 1.1 Aim of the thesis

Aerodynamic tools for accurate H-rotor simulations are studied in this thesis. The first step has been to get a better understanding of how the wind turbines are extracting power. The loads experienced by the blades have been then explored. A new simulation method has been developed and tested against experimental results. The goal has been to understand the different flow regimes during H-rotor operations in order to provide robust blade design. The method has been used to design several H-rotors. The new simulation method also provided the basis for the design of structural, mechanical and electrical components. The constructed H-rotors have been tested in representative real environment. The developed tools provides advanced modeling like aeroelastic coupling abilities, possibilities to simulate transient incoming winds and coupling with the turbine control system at a very reasonable computational cost on a normal PC. While the tool has been primarily developed for wind turbine applications, it can be applied to all kinds of vertical axis turbines.

The starting point for this thesis has been a past study of the H-rotor aerodynamics [5]. Parallel with the thesis, in the aerodynamic field, two Master thesis [6,7] and one 1-year traineeship report [8] have been completed using the model developed to design H-rotors. The work within the wind power group at the division for electricity and lightning has been performed as a team interacting with structural and electrical designers.

Several papers around the VAWT technical concept have also been published by the group related to the design of appropriate generators and controls [9, 10, 11, 12; 13, 14].

The main driver to investigate VAWT is to understand whether it can, in specific applications, be an alternative to the HAWT concept. The VAWT concept can reduce tower head mass which is a key element to access markets with constraints in crane availability. VAWTs show also promising aspects for cost efficient mass production and improved maintenance concepts.

## 1.2 Outline of the thesis

The thesis provides te general concepts of the new simulation methods and the context it was used in. The detailed elements have been documented in eight published papers.

The thesis is divided into 4 main sections:

- The concept studied in the thesis is presented in the current introduction.
- The second chapter gives some background on vertical axis turbines. These machines are used in the wind power sector but also in aeronautical and stream turbine applications. The challenges regarding the aerodynamic simulations are then presented.
- The third chapter gives the theory and semi analytical simulation method which has been developed to model the aerodynamics of a VAWT. Its last part considers the coupling of the model to investigate aeroelastic instabilities of H-rotors. Finally a short paragraph on low order methods is presented to complete the full range of methods needed for design purposes.
- The fourth chapter consists on a validation of the method against published and original experimental data.

Finally the last chapters include conclusions from the present work and suggestions for further developments

The eight papers are attached to the thesis as appendices.

- Paper I is a lemma to transform the physical rotor horizontal sections into a set of circles through conformal mapping.
- Paper II uses the simplified geometry of the circle to derive analytical solution for an unsteady blade in vertical axis motion.
- Paper III presents the generalization of the single blade approach to a full H-rotor with  $N$  blades.
- Paper IV introduces the coupling of the aerodynamic model to the elastic model of an H-rotor with transverse beams.

- Papers V to VIII are papers using the model developed in this thesis to design H-rotor type turbines and to analyze data produced from the turbines in both wind and underwater applications.

### 1.3 The concept

The overall design of the turbines studied in this thesis is a VAWT of the H-rotor type (see Fig 1) with straight blades supported with struts. The H-rotor is omni-directional and needs no yaw mechanism. Due to the straight blades, a simple blade profile can be used. The axis orientation enables the generator to be placed on the ground. The H-rotor concept studied here is of the direct drive type, i.e. the shaft is directly connected to the generator, thus eliminating the need for a gearbox. This concept enables a lighter tower structure. Furthermore, the H-rotor shows a lower optimal tip speed ratio limiting the noise emissions [15]. The use of electrical controlled passive stall regulation does not require pitching the blades. A detailed comparison between HAWTs and VAWTs can be found in [11].

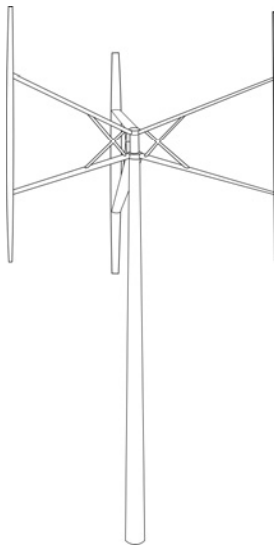


*Figure 1.* H- rotor : General view of an H-rotor with three blades



The overall strength of this concept lies in its operating simplicity. The table 2 below presents the H-rotor concept merits compared to conventional HAWTs

	HAWT	Direct drive H-rotor
Blade shape	--	+
Rotor mass	-	+
Generator mass	+	+(high but placed on ground)
Fatigue loads on rotor	-	--
Loads on tower	-	+
Loads on foundations	-	+
Fatigue loads on bearings	+	-
Gearbox system complexity	-	+(no gearbox)
Bearing system complexity	-	+
Yawing system complexity	-	+(none)
Pitching system complexity	-	+(none)
Braking system	+	-
Maintenance concept	-	+
Start up ability	+	-
Noise	-	+
Aerodynamics model accuracy	+	--

Table 2. Comparison between HAWTs and VAWTs, (+) marks a benefit, (-) a drawback

For the 500 kW range the total weight of the turbine is shown in [11] to be 30% times less than a conventional HAWT.

Conventional HAWTs (see Fig 2) have significant reliability and availability losses due to the gearbox, drive train and yaw system failures. These failures can be avoided with the direct drive H-rotor system. Operation and maintenance costs for this concept can be minimized under the conditions that VAWT's bearings and blades are designed in a robust manner.

### Failure Rate and Downtime from 2 Large Surveys of European Wind Turbines over 13 years

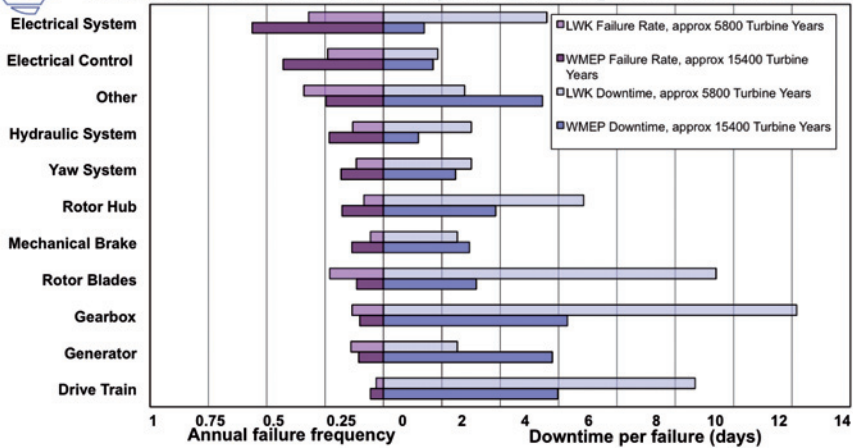


Figure 2. Failure rate and Downtime for conventional HAWTs systems with courtesy of ISET

The direct drive HAWT (for instance used in the Enercon concept) shows a higher mass compared to gearbox HAWTs. The H-rotor with generator and electronic system on the ground benefits from a lower top mass than conventional HAWTs. This has two advantages:

- More mass generates more cost. The low mass allows minimizing the turbine cost including the foundation cost.
- Optimization of installation costs. The H-rotor concept can access markets in developed countries with limited crane capacity. Thus limiting again the capital investment cost through cheaper installation.

The low tower head mass can be a crucial advantage for offshore applications or onshore applications in area with reduced crane availability. Their simplified structure can be used to optimize mass production costs for small or remote applications. The lack of mechanical control in conjunction with direct drive generators placed on the ground has the potential to substantially reduce the operation and maintenance costs. In summary the vertical axis turbines can represent a breakthrough for several applications.

## 2. Background

### 2.1 Historical overview of wind power and VAWTs

In this section a short historical overview of wind power with emphasis on the development of VAWTs is presented. An overview of the status of wind power in 2002, mainly focusing on HAWTs, is given in [16]. [17] provides an overview of wind turbine technologies with emphasis on HAWTs. A review of the development of horizontal and vertical axis wind turbines can be found in [18].

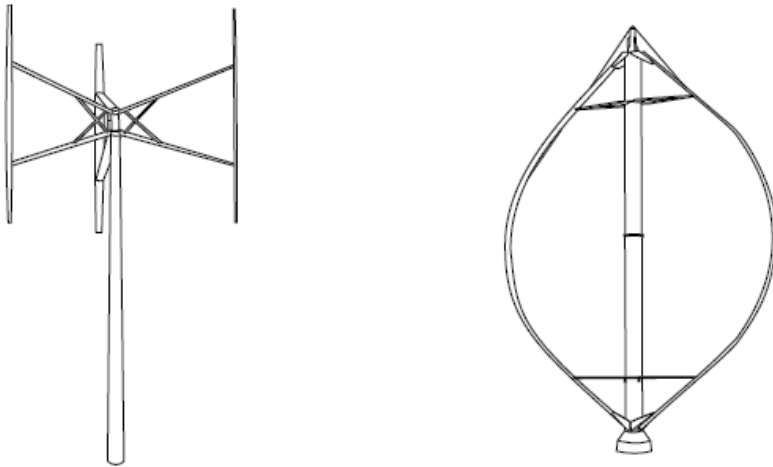


*Figure 3.* Basic VAWT configurations. To the left is a straight-bladed Darrieus rotor also known as H-rotor, and in the right is a Darrieus rotor.

The two main types of lift driven vertical axis turbines are shown in Fig 3. The Finnish engineer S.J. Savonius invented another type of drag base vertical axis wind turbine, the Savonius turbine in 1922, [19]. The Savonius rotor operates at high torques and low rotation speeds that are not favorable for electric power generation. The Savonius type of turbine will not be covered in the present study.

One of the first attempts to generate electricity by using the wind was made in the United States by Charles Brush in 1888 [20]. The turbine

developed by Marcellus Jacobs [20] was one of the most important early turbines. Jacobs' turbine had three airfoil shaped blades, battery storage and a wind wane keeping the turbine facing the wind. During the 20th century the horizontal axis wind turbines continued to evolve, which resulted in bigger and more advanced turbines, leading to the modern horizontal axis wind turbines [21].

Vertical axis turbines can also be used in ship propulsion as pioneered by Van Voith [22]. A modern development has been marketed by Voith Turbomarine GmbH company. The turbine uses variable pitch blades to create a thrust force on the desired direction improving its maneuverability.



*Figure 4. Voith Schneider propulsion concept with vertical axis technology [22]*

The same principle can be used in flight applications to generate both a thrust force and a lifting force. In this way, the wings can be replaced both in new airplanes concept and micro vehicle.

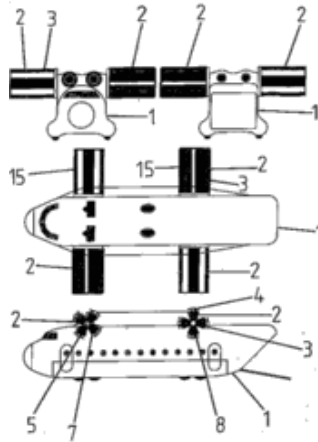


Figure 5. New airplane concept from patent [24]

The vertical axis turbine has also been applied to underwater applications both with fixed and pitching blades

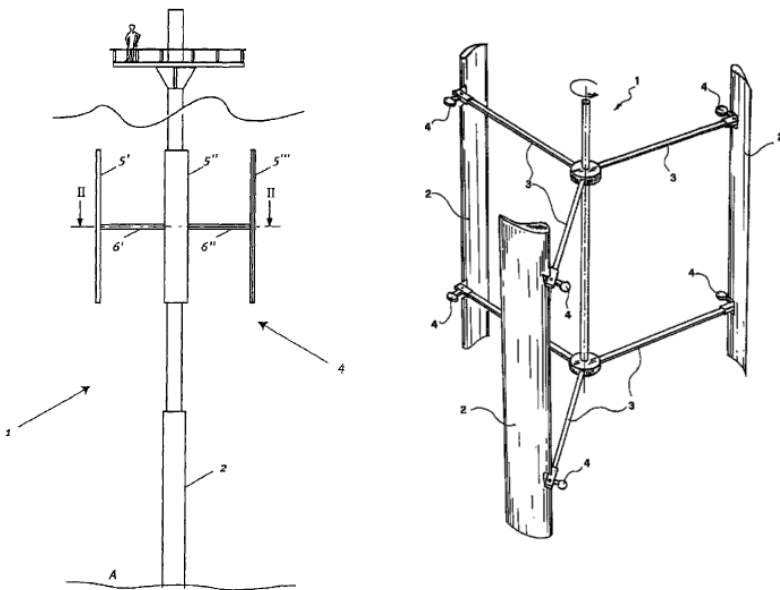


Figure 6. Underwater turbine vertical axis applications left [25] and right [26]

In wind applications, lift driven vertical axis wind turbines both with straight and curved blades have been invented by JM Darrieus in 1926 [27]. JM Darrieus patent also includes curved blades to avoid the bending due to centrifugal forces.

Several shapes have been used:

- Troposkein (shape taken by a rope in uniform rotation)
- Catenary (shape for a rope in rotation and in the gravitational field)
- Parabolic

Since Darrieus, judging from the hundreds of patents which have been developed, vertical axis wind turbines have been investigated with different support structures, arm connections and various blade section and blade shapes sometimes with an exotic taste.

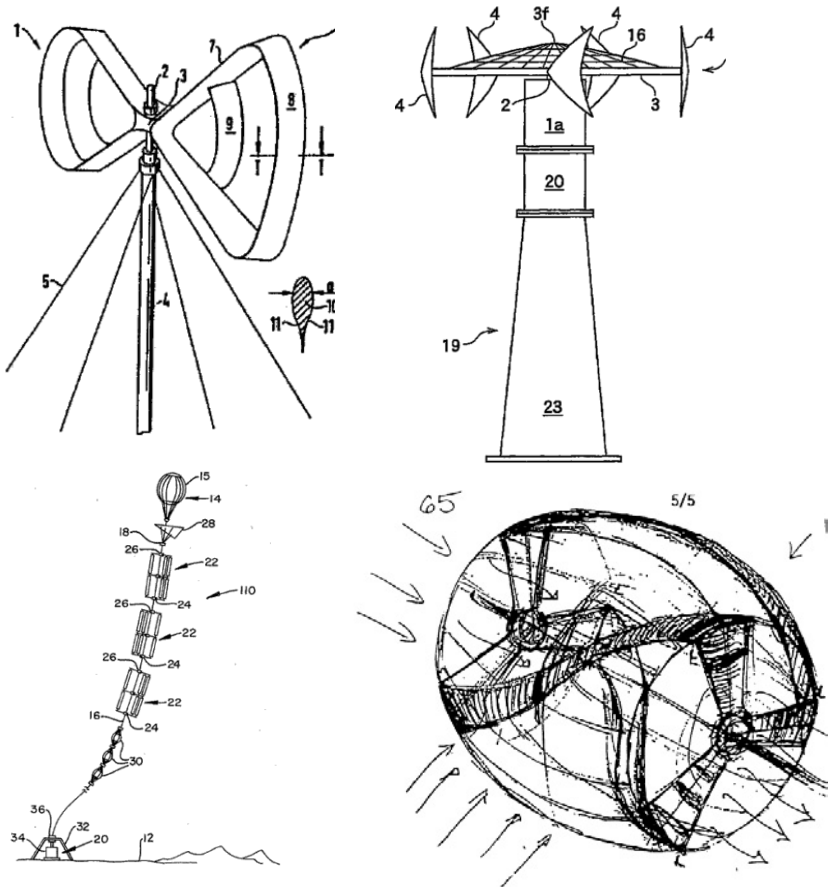


Figure 7. Various vertical axis wind turbine concepts from various patents [28, 29, 30, 31]

## 2.2 Working principle of VAWTs

The following paragraph will explain how the turbine under investigation creates its mechanical torque.

A horizontal section of a VAWT can be described with the following geometrical parameters (see Fig 8)

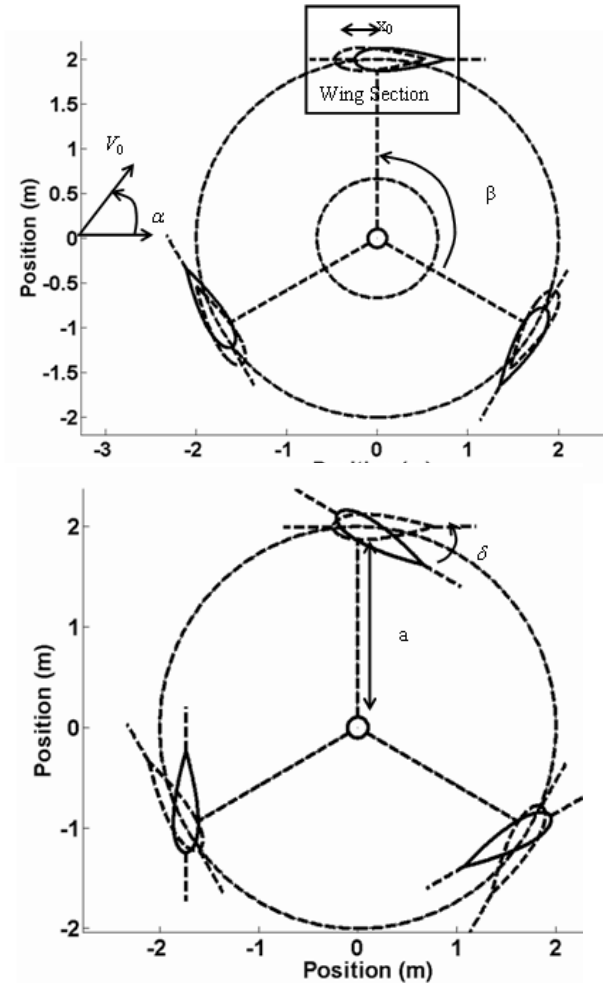


Figure 8. VAWT horizontal section basic geometry

Where

- $V_0$  is the asymptotic incoming wind speed,
- $\alpha$  the angle of the wind with respect to the X axis,
- $a$  is the rotor radius,
- $\delta$  the pitch angle,
- $x_0$  the blade shift position,
- $\beta$  the angular position of the blade at time t
- The wing section geometry will be described later on in details

In the following, we will use complex numbers to represent points of the plane as the blade position,  $z_{blade}$ . Only assuming in this principle explanation that  $\alpha = 0$  and that the flow velocity is not affected by the rotor motion.

$$z_{blade} = ae^{i\beta} \quad (2.1)$$

Assuming that the turbine is rotating at a constant speed  $\omega_R$ . The blade velocity vector in the complex plane will be given by

$$V_{blade} = ai \frac{d\beta}{dt} e^{i\beta} = i\omega_R z_{blade} \quad (2.2)$$

The relative wind seen by the blades will be given by the complex number

$$W_{seen} = V_0 - i\omega_R z_{blade} \quad (2.3)$$

The tangent vector along the blade is also given in its complex form by

$$T_{an} = iz_{blade} \quad (2.4)$$

It is possible from the previous parameters to form two one-dimensional parameters, the solidity  $s_{ol}$  and the tip speed ratio  $\lambda$  also called TSR

$$s_{ol} = \frac{Nc}{a} \quad (2.5)$$

$$\lambda = \frac{a\omega_R}{V_0} \quad (2.6)$$

In the above definition,  $c$  is the blade chord,  $N$  the number of blades. The angle of attack seen by the blade will be given by



$$\vartheta = A \cos\left(\frac{T_{an} \overline{W_{seen}}}{|T_{an}| |W_{seen}|}\right) \quad (2.7)$$

The horizontal bar above denotes the complex conjugate and the vertical bars the complex module of the two vectors defined in Eq. 2.3 and 2.4

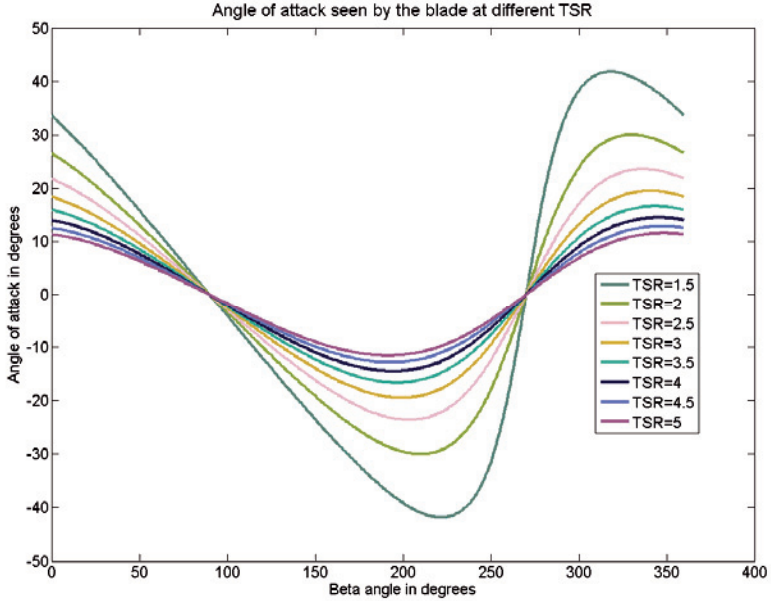


Figure 9. Relative angle of attack seen by the blades, TSR is the blade tip speed ratio

The angle of attack seen by the blade in the upwind region, represented by  $\beta$  angles between  $90^\circ$  to  $270^\circ$  is negative, see Fig 9. On the blade section, a lift force will be created perpendicular to the relative wind speed. This force will be pointing to the inside of the rotor circle. It can be decomposed into a component along the tangent to the blade and a component perpendicular to the blade. The tangential force gives the rotor torque. The perpendicular force gives the normal forces. The forces are usually presented as undimensional force.

The angle of attack seen by the blade is positive on the downwind side of the rotor, represented by  $\beta$  angles less than  $90^\circ$  and more than  $270^\circ$ . The lift force perpendicular to the relative wind speed will be pointing to the outside of the rotor circle.

Both upwind and downwind parts contribute to the torque creation assuming no perturbation to the flow due to the turbine. The normal forces sums up to mainly create a thrust along the wind direction.

The normal and tangential forces coefficient are defined as

$$C_T = \frac{T_f}{\frac{\rho}{2} V_0^2 c}, \quad C_N = \frac{N_f}{\frac{\rho}{2} V_0^2 c}, \quad (2.8)$$

where  $T_f$  is the tangential force in N,  $\rho$  is the fluid mass density,  $N_f$  the normal force in N,  $c$  the airfoil section chord.

It will be seen in the following that the effect of continuously changing angles of attack induces a continuously changing circulation on the blades which generates a vortex formation as described by Kelvin's theorem [32]. These vortices are strongly disturbing the flow especially in the downwind part.

## 2.2 Aerodynamic efficiency measures

The power produced by a wind turbine is absorbed from the kinetic energy in the wind. It is thus proportional to the projected frontal area  $A$  of the turbine. In aerodynamics this area is sometimes called the swept area of the turbine according to the terminology derived from the HAWTs. A wind turbine cannot capture all kinetic energy of the wind. If so the air would come to a standstill behind the turbine. Accordingly it is reasonable to assume an upper limit for the aerodynamic efficiency which is less than one. The so called Betz' limit of (59 %) is mentioned as this maximum. The technical name for aerodynamic efficiency of a wind turbine is the power coefficient defined as:

$$C_p = \frac{P_m}{\frac{1}{2} \rho A V_0^3} \quad (2.9)$$

where  $P_m$  is the power produced,  $V_0$  is the wind speed and  $A$  is the projected frontal area of the turbine.

Modern HAWTs have evolved during many years of research and experience. The aerodynamic efficiency is close to 50% whereas VAWTs do not exceeded 40%. Even so, there is no decisive argument why VAWTs should be less efficient than HAWTs. On the contrary, the VAWTs sweep the area twice, opening a theoretical possibility of reaching  $C_p$  exceeding the

Betz limit [33]. On the other hand, there are sections of the lap where the blades can not produce a positive torque. Furthermore the blades are forced to move through the turbulent wake on the downwind part of a revolution. This could induce rapid fluctuations in the blade loads and increase drag. More important, efficiency aside, turbines must be constructed to function properly for the intended lifetime of the device. This means vertical axis turbines need to be designed for reduced load fluctuations on the blades and shaft. For example the curved blades of Darrieus vertical axis wind turbines were known to fail from fatigue as early as two years after construction. The emergence of modern materials has somewhat relieved this situation. Nevertheless how to decrease the variance in the load is still an open question.

The cost of high performance construction material like carbon fiber is very high. Making decrease use of these materials is a high priority for improved economy. It is hence important when designing VAWTs to correctly understand the structure of the flow and how it corresponds to the blade loads.

## 2.3 Current VAWT projects

Currently the market is dominated by the horizontal axis turbines. However, there is no lack of interest in the vertical axis concept. In fact, the vertical axis turbines have received close attention, especially in the academic community.

The VAWT concept has improved with research. The largest research effort to date was done by Sandia National Laboratories (SNL) in USA leading to a wide number of pioneering research and publications [34, 35]. SNL routinely built and studied curved bladed Darrieus turbines over fifteen years.

Canada and Great Britain also financed large scale research projects on VAWTs (see Fig 10). Commercial turbines were produced for example by FloWind in USA; by VAWT Ltd. in Britain (see Fig 10 right) and by Heidelberg in Germany (Fig 11). Important to note, all these first-of-a-kind turbines did not last for their full designed lifetime due to bearing or blade failure.






*Figure 10. Eole turbine in Canada (left) and H rotor in UK (right)*



*Figure 11. Heidelberg rotor Germany*

Increased market for wind turbines in conjunction with the current climate concerns has sparked recent development notably opening a new niche for VAWTs in city surroundings. For example the Dutch company Turby is marketing its machines for use in turbulent environments where the wind direction changes often emphasizing that the VAWT is insensitive to change in wind direction. In Table 4, some current commercial (or close to coming to market) products are listed.

Product	Product name	Power range	Concept	Country	<i>N</i>
	Ropatec	To 6 kW	Straight blades	Italy	2
	Dermond	100 kW	Curved blades	Canada	3
	Solwind	2-10 kW	Straight blades	New Zealand	2




Product	Product name	Power range	Concept	Country	<i>N</i>
	Turby	2.5 kW	Straight blades with twist	The Netherlands	3
	XCO2	6 kW	Straight blades with twist	UK	3
	Neuhauser	to 40 KW	Straight blades	Germany	3

Table 3. Closest to market VAWTs products

## 2.4 Aerodynamic specificities of H-rotor flows

The simulation method described in section 3 below has been developed with emphasis on two peculiarities of cross flow turbines: the complicated flow surrounding vertical turbines and the sensitive dependency on various aerodynamic parameters. Which key physical features need to be investigated in detail depend on turbine operations with features' importance varying with the Tip Speed Ratio TSR:

For all TSRs:

- Unsteady interaction between the blades due to the continuously changing angle of attack via vortex shedding leading to complicated wake structures (see Fig 11). The number of times one airfoil going through the downwind pass crosses a wake depends on the TSR

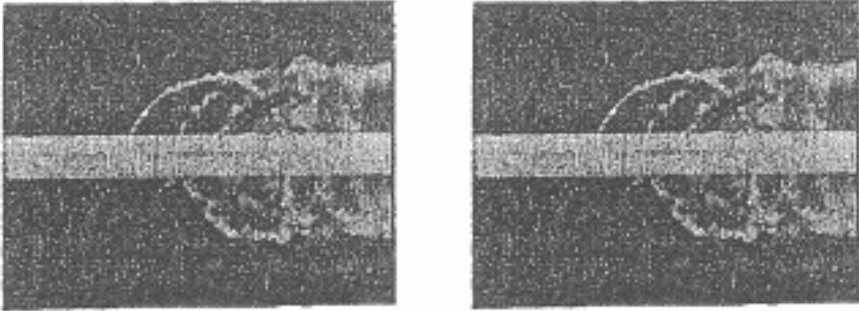


*Figure 11.* Wake development for two straight bladed VAWTs at low and medium TSRs [35]

- 3 dimensional effects such as tip effects in case of low aspect ratio wings (ratio of the blade length over the blade chord) and wind shear effects
- Unsteady relative flow curvature experienced by the blades during rotation especially for high solidity concepts
- As for all other wind turbines, dynamic changes in wind directions and turbulence eddies are difficult to model.

For low TSRs

- Dynamic stall phenomenon (see Fig 12)

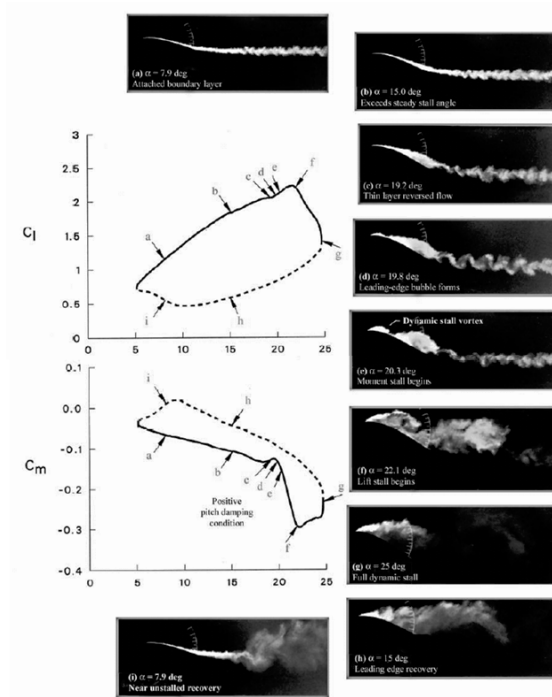


Figure 12. Typical flow and Lift and pitching moment impact for a foil pitching at high angles of attack.

- Viscous effects and the continuous change of Reynolds numbers over each turns

For high TSRs

- Secondary effects of cross arms
- Tower shadow

## 2.5 Benefit and drawbacks of aerodynamic approaches

In the past there have been several attempts to modeling lift-driven VAWTs each with its own advantages and disadvantages. The different methods can be classified in six groups:

1. Analytical aerodynamic efficiency predictions
2. Fixed-wake vortex models
3. Streamtube models
4. Direct Numerical Simulations
5. Large Eddy Simulations
6. Free-wake vortex models



The first of the two analytical efficiency prediction models is the double actuator disc model [36]. One can conceive it as two Betz turbines in tandem with some spacing in-between. Newman showed that the maximum  $C_p$  of such a double actuator-disc system is  $C_p = 16/25 = 64\%$  [36].

The other semi-analytical attempt is the so-called fixed-wake vortex model developed by Holme [37] and extended by Fanucci et al [38]. This model assumes an infinite number of wings but with a solidity fixed to a given value. Each wing at azimuth angle position has some circulation around it. This circulation is calculated from the local angle of attack. Hence the vortex sheet bounds the turbine. Due to the change in circulation between adjacent wings, there are also vortex sheets which leave the turbine. This sheet is modeled to be convected downstream at a uniform velocity. Thus the blade forces can be calculated from Kutta-Joukowski principle and integrated to obtain the performance of the turbine.

Streamtube models are the most popular for prediction of performance. They are the analogous of the Blade Element Momentum (BEM) methods, which are the most common tool for HAWT aerodynamic analysis. There exists a full range of models which vary in how detailed the analysis is. The most sophisticated streamtube model is the Double Multiple Streamtube model (DMST) due to Paraschivoiu [39] and Homicz [40]. The first streamtube model was developed by Templin in 1974 [41]. In brief the flow is modeled as composed by a grid of linear streamtubes. Static airfoil data is used for each streamtube to calculate the average blade forces from lift and drag using the relative velocity to calculate the angle of attack and blade Reynolds number. This average force is used to calculate the loss of momentum and thus the slowdown of the wind. The models can not predict the structure of the wake but are on the other hand extremely fast and can with advantage be used for quick back-of-the-envelope calculations of blade forces and turbine performance. Important effects like dynamic stall are included via empirical formulas and corrections. Therefore the main drawback of these streamtube models is the shortage of airfoil data in VAWT operations to feed in the models. In other words, these models are good for a detailed design of the turbine as far as no innovative options are used.

In terms of thoroughness the streamtube models has its opposite in the method of direct numerical simulation (DNS). In DNS the Navier-Stokes equations are solved numerically with some PDE-solving method such as Finite Elements (FEM) or Finite Volumes (FVM) using a fine enough grid to capture all relevant effects. In theory this approach can be used to investigate all aspects of the turbine aerodynamics. However, in practice, the large computational costs associated with such methods limits their use to specific details such as dynamic stall modeling and even these applications come at a large computational cost.

Various authors, notably Ferreira et al have used Large Eddy Simulations (LES) to study the effect of dynamic stall [42, 43]. The drawback, as with DNS, is that detailed simulations long enough for the wake to develop completely are very expensive computationally. However, a recent article by Lida [44] shows promising development in this direction.

The last group of models, used in this thesis falls into free vortex methods. The lift force of a blade in Darrieus motion is due to the circulation building up around the blade. However, since the lift and thus the circulation is changing during a revolution, a continuous line of eddies are shed from each wing in order to conserve the angular momentum of the air. “Discrete Vortex Methods” model this line into separate eddies and tracks the resulting eddies as they are convected downstream. The first vortex simulations of Darrieus turbines in inviscid flow were performed by Strickland [35]. It was based on the principle of a lifting line approach using airfoil data sheets to calculate the circulation. Lifting line approaches have since then been the most popular of the vortex models. Another possibility is to use panel methods with the advantage to simulate the behavior of general airfoils. However, the panel methods become soon computationally intensive with the wake development.

In summary, vortex methods are well fitted for highly complex vortex flow experienced in VAWT (see Fig 11). The diversity of free vortex methods depends on:

- The model dimension: two or three dimensional
- The way of treating the wake using continuous vortex lines or discrete vortex points.
- The source used to derive the airfoil circulation: i.e. is it data based or calculated. If calculated it can be assessed via
- Analytical methods like conformal mapping ones
- Panel methods
- CFD methods

## 3. Semi analytical theory of unsteady aerodynamics

### 3.1 Equations

The aim of this paragraph is to find a computationally efficient and accurate method to evaluate the unsteady forces from the fluid flow into the blades or wings. The unsteady forces on the blades depend on the pressure field around the blades as well as friction forces which depends on the fluid velocity profile at the blade vicinity.

Finding all flow quantities requires solving the fluid flow equations with special boundary conditions both at infinity and at the blade sections. This set of equation together with its boundary conditions are referred to as the fluid flow problem.

Various quantities of the flow such as flow velocity, vorticity and pressure should be evaluated. Theses flow quantities are governed by two main fluid flow equations:

- Mass conservation see section 3.1.1
- Navier Stokes equations see section 3.1.2

These equations are valid inside the fluid area. They consist in non linear PDEs and should then be completed by some boundary conditions. These boundary conditions are derived in section 3.2.

The idea of the methodology derived here is to assume inviscid and incompressible two dimensional flows. The flow is split into two different parts. The flow is rotational in specific areas modeled by special kernels (see section 3.1.1). These rotational areas deforms following the vorticity transport equations derived from the Navier Stokes equations in 3.1.3. Apart in these areas commonly called the wake, the flow streamfunction around an H-rotor can be found analytically at each time step if the boundary conditions are simplified. The aim of section 3.3 is to find a methodology to transform a set of sections into a set of circles. This then simplifies enough the boundary conditions to derive the analytical solution. Once the full streamfunction is known analytically at each time step, all necessary quantities for the computation of the Bernoulli equations (see section 3.1.4) are also known and the forces can be also derived analytically (see section 3.4.5)

Although the following standard fluid equations are usually written in terms of Cartesian or polar coordinates, special features of analytic function suggest to start writing the general fluid internal equations in the form of function of a complex number  $s$  and  $\bar{s}$  its complex conjugate.

### 3.1.1. Mass conservation

The conservation of mass writes:

$$\frac{d\rho}{dt} = 0 \quad (3.1a)$$

where  $\rho$  is the mass density of the fluid considered, the operator  $d/dt$  is called the Lagrangian derivative or the material derivative, it corresponds to the derivative of the field with respect to time if the field is expressed in Lagrangian coordinates (following one fluid particle). In eulerian variables, mass conservation reads

$$\frac{\partial \rho}{\partial t} + \underline{\nabla} \cdot (\rho \underline{U}) = 0 \quad (3.1b)$$

$\underline{U}$  is the velocity field expressed in Eulerian coordinates (looking at the fluid at one instant). The underscore denotes vectors. It is now assumed that the eulerian density of the fluid is constant both in time and space (incompressible flow assumption, a good approximation for wind turbines but not for supersonic aircraft for instance). The previous equation can be rewritten as:

$$\underline{\nabla} \cdot (\underline{U}) = 0 \quad (3.2)$$

or in other terms  $div(\underline{U}) = 0$

In two dimensions  $\underline{U} = (U_x, U_y)$  rewritten in complex variables notation and using the complex conjugate:

$$\underline{U} = U_x + iU_y = \frac{U + \bar{U}}{2} + i \frac{U - \bar{U}}{2i} \quad (3.3a)$$

The velocity is considered as

$$\underline{U}(x, y) = V(s, \bar{s}) \quad (3.3b)$$

where  $s = x + iy$  is a generic complex number with real part  $x$  and imaginary part  $y$ .  $V$  is a function of the complex plane into the complex plane. The divergence of the fluid velocity is then

$$div(\underline{U}) = \frac{\partial U_x}{\partial x} + \frac{\partial U_y}{\partial y} \quad (3.4a)$$

So in terms of complex number

$$\text{div}(\underline{U}) = \frac{1}{2} \left\{ \frac{\partial(V(s, \bar{s}) + \bar{V}(s, \bar{s}))}{\partial x} - i \frac{\partial(V(s, \bar{s}) - \bar{V}(s, \bar{s}))}{\partial y} \right\}, \quad (3.4b)$$

where by definition, the function  $\bar{V}(s, \bar{s}) = \overline{V(s, \bar{s})}$

Thus the divergence Eq 3.4b transforms into:

$$\text{div}(\underline{U}) = \frac{1}{2} \left\{ \begin{array}{l} \frac{\partial V}{\partial s} + \frac{\partial V}{\partial \bar{s}} + \frac{\partial \bar{V}}{\partial s} + \frac{\partial \bar{V}}{\partial \bar{s}} + \dots \\ \dots \frac{1}{i} \left[ i \frac{\partial V}{\partial s} - i \frac{\partial V}{\partial \bar{s}} - i \frac{\partial \bar{V}}{\partial s} + i \frac{\partial \bar{V}}{\partial \bar{s}} \right] \end{array} \right\} \quad (3.4c)$$

or,

$$\text{div}(\underline{U}) = \frac{1}{2} \left\{ \begin{array}{l} \frac{\partial V}{\partial s} + \frac{\partial V}{\partial \bar{s}} + \frac{\partial \bar{V}}{\partial s} + \dots \\ \dots \frac{\partial \bar{V}}{\partial s} + \frac{\partial V}{\partial s} - \frac{\partial V}{\partial \bar{s}} - \frac{\partial \bar{V}}{\partial s} + \frac{\partial \bar{V}}{\partial \bar{s}} \end{array} \right\} \quad (3.4d)$$

Simplifying gives

$$\text{div}(\underline{U}) = \frac{\partial V}{\partial s} + \frac{\partial \bar{V}}{\partial \bar{s}} \quad (3.4e)$$

From the definition of the function  $\bar{V}$ , it is noted that  $\frac{\partial \bar{V}}{\partial s} = \frac{\partial \bar{V}}{\partial \bar{s}}$  and thus

$$\text{div}(\underline{U}) = 2 \text{Re} \left( \frac{\partial V}{\partial s} \right) \quad (3.4f)$$

In conclusion a complex velocity field is incompressible if and only if

$$\text{div}(\underline{U}) = \frac{\partial V}{\partial s} + \frac{\partial \bar{V}}{\partial \bar{s}} = 0 \quad (3.4g)$$

### Vorticity and stream function

The vorticity is defined as the quantity:

$$\underline{\omega} = \text{curl}(\underline{U}) = \nabla \times \underline{U} \quad (3.5)$$

And for a two dimensional flow, the vorticity vector is along the last axis.

$$\omega = \text{curl}(\underline{U})|_z \quad (3.6a)$$

where  $\omega$  is the complex vorticity. The vorticity can also be expressed in terms of a real function of a complex field. The same procedure as for the mass conservation equation allows the complex vorticity to be expressed as:

$$\omega = \frac{1}{i} \left\{ \frac{\partial V}{\partial s} - \frac{\partial \bar{V}}{\partial \bar{s}} \right\} = 2 \operatorname{Im} \left( \frac{\partial V}{\partial s} \right) \quad (3.6b)$$

The term  $\frac{\partial V}{\partial s}$  expresses both the compression and the rate of rotation of the fluid.

If the two dimensional flow is incompressible, the curl takes the form

$$\omega = \frac{2}{i} \frac{\partial V}{\partial s} \quad (3.6c)$$

The coherent definition of the stream function will be

$$V(s, \bar{s}) = \operatorname{curl}(\psi \underline{e}_z) = -2i \frac{\partial \psi}{\partial s}$$

Once the stream function is known, the velocity field and also the vorticity can be deduced easily by using mass conservation:

$$\omega = \frac{1}{i} \left\{ \frac{\partial V}{\partial s} - \frac{\partial \bar{V}}{\partial \bar{s}} \right\} = \frac{2}{i} \frac{\partial V}{\partial s} = -2i \frac{\partial V}{\partial s} \quad (3.6d)$$

$$\omega = -4 \frac{\partial}{\partial s} \left( \frac{\partial \psi}{\partial \bar{s}} \right) = -4 \frac{\partial^2 \psi}{\partial s \partial \bar{s}} \quad (3.6e)$$

For a scalar field  $\Delta \psi = 4 \frac{\partial^2 \psi}{\partial s \partial \bar{s}}$  where  $\Delta = \partial^2 / \partial x^2 + \partial^2 / \partial y^2$  is the

Laplacian thus

$$\omega = -\Delta \psi \quad (3.6f)$$

which is Poisson's equation. The vorticity is in general a non-linear function dependent on the flux function in a complicated manner, whereby a construction of a solution to the Poisson equation for two-dimensional flows becomes a sophisticated task. Therefore, when the stream function is known, the velocity field and the vorticity distribution are also known. Additionally to introduce a non zero vorticity in the flow, the stream function  $\psi$  should depend both on  $s$  and on  $\bar{s}$ . Furthermore if a velocity field is given analytically as a function of  $s$  and  $\bar{s}$ , the stream function can be obtained via a simple integration with respect to  $\bar{s}$ . The additive function of  $s$  is found from the demand that the stream function should be real.

### Examples of two useful stream functions

- The Rankine vortex centered in the complex point  $s_V$  is defined by a tangential velocity only

$$\left\{ \begin{array}{l} V_\theta = \left( \frac{\Gamma_V}{2\pi r_C} \frac{|s - s_V|}{r_C} \right), 0 \leq |s - s_V| \leq r_C \\ V_\theta = \left( \frac{\Gamma_V}{2\pi r_C} \frac{r_C}{|s - s_V|} \right), r_C \leq |s - s_V| \end{array} \right. \quad (3.7a)$$

where  $V_\theta$  is the tangential real velocity,  $\Gamma_V$  the vortex circulation,  $s_V$  the complex number representing the vortex position and  $r_C$  the vortex radius. It gives for the velocity field expressed in complex variables

$$\left\{ \begin{array}{l} V(s, \bar{s}) = \left( \frac{i\Gamma_V}{2\pi r_C} \frac{s - s_V}{r_C} \right), 0 \leq |s - s_V| \leq r_C \\ V(s, \bar{s}) = \left( \frac{i\Gamma_V}{2\pi r_C} \frac{r_C}{s - s_V} \right), r_C \leq |s - s_V| \end{array} \right. \quad (3.7b)$$

Thus the associated stream function will be:

$$\left\{ \begin{array}{l} \psi(s, \bar{s}) = -\left( \frac{\Gamma_V}{4\pi r_C} \frac{(s - s_V)(\bar{s} - \bar{s}_V)}{r_C} \right), 0 \leq |s - s_V| \leq r_C \\ \psi(s, \bar{s}) = -\left( \frac{\Gamma_V}{4\pi r_C} r_C \log(|s - s_V|^2) \right), r_C \leq |s - s_V| \end{array} \right. \quad (3.8)$$

$\psi$  is a radial function only in this case. The corresponding vorticity is

$$\left\{ \begin{array}{l} \omega(s, \bar{s}) = \left( \frac{\Gamma_V}{\pi r_C} \frac{1}{r_C} \right), 0 \leq |s - s_V| \leq r_C \\ \omega(s, \bar{s}) = 0, r_C \leq |s - s_V| \end{array} \right. \quad (3.9)$$

This model gives a jump in the vorticity at the core limit.

The flow is irrotational far from the vortex center or outside the vortex core and also incompressible by assumption (i.e. ideal). The corresponding complex potential (which exist only for an ideal flow) will be

$$F(s, \bar{s}) = \frac{-i\Gamma_V}{2\pi} \frac{1}{s - s_V}, r_C \leq |s - s_V| \quad (3.10)$$

We have rederived the classical expression for the velocity from the complex potential for an ideal flow.

- *The Lamb-Oseen vortex* which is a smoothed form of the Rankine vortex has its velocity given by:

$$V_{\theta} = \frac{\Gamma_V}{2\pi|s - s_V|} \left( 1 - e^{-\beta \frac{|s - s_V|^2}{r_c^2}} \right) \quad (3.11a)$$

where  $V_{\theta}$  is the tangential real velocity,  $\Gamma_V$  the vortex circulation,  $s_V$  the complex number representing the vortex position,  $r_c$  a measure of the vortex radius and  $\beta$  a constant.

This gives the velocity field expressed in complex variables

$$V(s, \bar{s}) = \frac{i\Gamma_V}{2\pi(\bar{s} - s_V)} \left( 1 - e^{-\beta \frac{|s - s_V|^2}{r_c^2}} \right) \quad (3.11b)$$

and thus the associated stream function is:

$$\psi(s, \bar{s}) \equiv -\frac{\Gamma_V}{4\pi} \left( \log(|s - s_V|^2) + E_1 \left( \beta \frac{|s - s_V|^2}{r_c^2} \right) \right) \quad (3.12)$$

with  $E_1(X) = \lim_{A \rightarrow \infty} \int_X^A \frac{e^{-u}}{u} du$

The last expression shows that the stream function is a radial function also in this case. The vorticity becomes

$$\omega(s, \bar{s}) = \frac{\beta\Gamma_V}{\pi r_c^2} e^{-\beta \frac{|s - s_V|^2}{r_c^2}} \quad (3.13)$$

and the circulation contained in a cylinder of radius  $r'$  is

$$\Gamma(r') = \Gamma_V \left( 1 - e^{-\beta \frac{r'^2}{r_c^2}} \right) \quad (3.14)$$

The circulation far from the vortex center quickly converges to the ideal Dirac point vortex result.

The potential for the Lamb Oseen vortex is well defined and can be rewritten as:

$$\psi(s, \bar{s}) = -\frac{\Gamma_V}{4\pi} \left( -\sum_{k=0}^{+\infty} \frac{(-1)^{k+1}}{(k+1)!(k+1)} \left( \beta \frac{|s - s_V|^2}{r_c^2} \right)^{k+1} \right). \quad (3.15)$$



This form has a limit in  $s \rightarrow s_\nu$  which was not obvious from the definition. This form tends to the Green's function when far from the core.

### 3.1.2. Navier Stokes equations

Using the same procedures as above, the full Navier Stokes equations can be rewritten in the simplified complex form:

$$\frac{\partial V}{\partial t} + V \frac{\partial V}{\partial s} + \bar{V} \frac{\partial V}{\partial \bar{s}} = -2 \frac{\partial p}{\partial s} + \frac{4}{R_e} \frac{\partial^2 V}{\partial s \partial \bar{s}} \quad (3.16)$$

where  $p$  is the pressure field inside the fluid and  $R_e$  is the Reynolds number quantifying the effects of inertia forces against viscous forces. For an ideal inviscid flow the Reynolds number tends to infinity.

In the special case of an ideal inviscid, irrotational incompressible flow:

$$\omega = \frac{2}{i} \frac{\partial V}{\partial s} = 0 \Rightarrow \frac{\partial V}{\partial s} = 0 \quad (3.17)$$

The Navier Stokes equations take the form of the ideal equations:

$$\frac{\partial V}{\partial t} + \bar{V} \frac{\partial V}{\partial \bar{s}} = -2 \frac{\partial p}{\partial \bar{s}} \quad (3.18a)$$

### 3.1.3. Vorticity and vorticity transport

To obtain the equation for the vorticity, the curl operator is applied to the Navier Stokes equations written in complex coordinates form. The Navier Stokes equations are first differentiated with respect to  $s$

$$\begin{aligned} \frac{\partial}{\partial s} \frac{\partial V}{\partial t} + \frac{\partial}{\partial s} \left( V \frac{\partial V}{\partial s} + \bar{V} \frac{\partial V}{\partial \bar{s}} \right) &= -2 \frac{\partial}{\partial s} \frac{\partial p}{\partial \bar{s}} \\ &+ \frac{4}{R_e} \frac{\partial}{\partial s} \frac{\partial^2 V}{\partial s \partial \bar{s}} \end{aligned} \quad (3.18b)$$

Taking the conjugate of the Navier Stokes equations and differentiating it with respect to  $\bar{s}$

$$\begin{aligned} \frac{\partial}{\partial \bar{s}} \frac{\partial \bar{V}}{\partial t} + \frac{\partial}{\partial \bar{s}} \left( \bar{V} \frac{\partial \bar{V}}{\partial \bar{s}} + V \frac{\partial \bar{V}}{\partial s} \right) &= -2 \frac{\partial}{\partial \bar{s}} \frac{\partial p}{\partial s} \\ &+ \frac{4}{R_e} \frac{\partial}{\partial \bar{s}} \frac{\partial^2 \bar{V}}{\partial \bar{s} \partial s} \end{aligned} \quad (3.18c)$$

At the end by taking the difference of these two Eq 3.18b and 3.18c, looking at each of the terms and using that by definition of the vorticity for an incompressible flow:

$$\omega = \frac{2}{i} \frac{\partial V}{\partial s} \quad (3.19)$$

$$\frac{\partial}{\partial s} \frac{\partial V}{\partial t} = \frac{\partial}{\partial t} \left( \frac{\partial V}{\partial s} \right) = \frac{i}{2} \frac{\partial \omega}{\partial t} \quad (3.20)$$

And using the incompressibility

$$\frac{\partial}{\partial \bar{s}} \frac{\partial \bar{V}}{\partial t} = \frac{\partial}{\partial t} \left( \frac{\partial \bar{V}}{\partial \bar{s}} \right) = -\frac{\partial}{\partial t} \left( \frac{\partial V}{\partial s} \right) = -\frac{i}{2} \frac{\partial \omega}{\partial t} \quad (3.21)$$

For the convection terms:

$$\begin{aligned} \frac{\partial}{\partial s} \left( V \frac{\partial V}{\partial s} + \bar{V} \frac{\partial V}{\partial \bar{s}} \right) &= \frac{\partial V}{\partial s} \frac{\partial V}{\partial s} \\ &+ V \frac{\partial^2 V}{\partial s^2} + \frac{\partial \bar{V}}{\partial s} \frac{\partial V}{\partial \bar{s}} + \bar{V} \frac{\partial^2 V}{\partial s \partial \bar{s}} \end{aligned} \quad (3.22)$$

and also that:

$$\begin{aligned} \frac{\partial}{\partial \bar{s}} \left( \bar{V} \frac{\partial \bar{V}}{\partial \bar{s}} + V \frac{\partial \bar{V}}{\partial s} \right) &= \frac{\partial \bar{V}}{\partial \bar{s}} \frac{\partial \bar{V}}{\partial \bar{s}} \\ &+ \bar{V} \frac{\partial^2 \bar{V}}{\partial \bar{s}^2} + \frac{\partial V}{\partial \bar{s}} \frac{\partial \bar{V}}{\partial s} + V \frac{\partial^2 \bar{V}}{\partial \bar{s} \partial s} \end{aligned} \quad (3.23)$$

Using the incompressibility (the field  $V$  is divergence free):

$$\begin{aligned} \frac{\partial}{\partial \bar{s}} \left( \bar{V} \frac{\partial \bar{V}}{\partial \bar{s}} + V \frac{\partial \bar{V}}{\partial s} \right) &= \frac{\partial V}{\partial s} \frac{\partial V}{\partial s} \\ -\bar{V} \frac{\partial^2 V}{\partial \bar{s} \partial s} + \frac{\partial V}{\partial \bar{s}} \frac{\partial \bar{V}}{\partial s} + V \frac{\partial^2 \bar{V}}{\partial \bar{s} \partial s} \end{aligned} \quad (3.24)$$

And now considering

$$\begin{aligned} A(s, \bar{s}, t) &= \frac{\partial}{\partial s} \frac{\partial V}{\partial t} + \frac{\partial}{\partial s} \left( V \frac{\partial V}{\partial s} + \bar{V} \frac{\partial V}{\partial \bar{s}} \right) \\ &- \frac{\partial}{\partial \bar{s}} \frac{\partial \bar{V}}{\partial t} - \frac{\partial}{\partial \bar{s}} \left( \bar{V} \frac{\partial \bar{V}}{\partial \bar{s}} + V \frac{\partial \bar{V}}{\partial s} \right) \end{aligned} \quad (3.25a)$$

From the previous equations:

$$\begin{aligned} A(s, \bar{s}, t) &= \frac{i}{2} \frac{\partial \omega}{\partial t} + \frac{i}{2} \frac{\partial \omega}{\partial t} + \frac{\partial V}{\partial s} \frac{\partial V}{\partial s} + V \frac{\partial^2 V}{\partial s^2} \\ &+ \frac{\partial \bar{V}}{\partial s} \frac{\partial V}{\partial \bar{s}} + \bar{V} \frac{\partial^2 V}{\partial s \partial \bar{s}} - \frac{\partial V}{\partial s} \frac{\partial V}{\partial s} \\ &+ \bar{V} \frac{\partial^2 V}{\partial \bar{s} \partial s} - \frac{\partial V}{\partial \bar{s}} \frac{\partial \bar{V}}{\partial s} - V \frac{\partial^2 \bar{V}}{\partial \bar{s} \partial s} \end{aligned} \quad (3.25b)$$

Thus, simplifying

$$A(s, \bar{s}, t) = i \frac{\partial \omega}{\partial t} + V \frac{\partial^2 V}{\partial s^2} - V \frac{\partial^2 \bar{V}}{\partial \bar{s} \partial s} + 2\bar{V} \frac{\partial^2 V}{\partial s \partial \bar{s}} \quad (3.25c)$$

Using that the incompressibility and that the vorticity or quasi vorticity is a scalar and is related to the derivatives of the velocity field by  $\frac{\partial V}{\partial s} = \frac{i\omega}{2}$  but

also  $\frac{\partial \bar{V}}{\partial \bar{s}} = \frac{-i\omega}{2}$ . Replacing these expressions in the previous ones

$$A(s, \bar{s}, t) = i \frac{\partial \omega}{\partial t} + \frac{i}{2} V \frac{\partial \omega}{\partial s} + \frac{i}{2} V \frac{\partial \omega}{\partial s} + i \bar{V} \frac{\partial \omega}{\partial \bar{s}} \quad (3.25d)$$

$$A(s, \bar{s}, t) = i \left[ \frac{\partial \omega}{\partial t} + V \frac{\partial \omega}{\partial s} + \bar{V} \frac{\partial \omega}{\partial \bar{s}} \right] \quad (3.25e)$$

And from the Navier Stokes equations:

$$A(s, \bar{s}, t) = -2 \frac{\partial}{\partial s} \frac{\partial p}{\partial \bar{s}} + \frac{4}{\text{Re}} \frac{\partial}{\partial s} \frac{\partial^2 V}{\partial s \partial \bar{s}} + 2 \frac{\partial}{\partial \bar{s}} \frac{\partial p}{\partial s} - \frac{4}{R_e} \frac{\partial}{\partial \bar{s}} \frac{\partial^2 \bar{V}}{\partial s \partial \bar{s}} \quad (3.25f)$$

$$A(s, \bar{s}, t) = \frac{4}{R_e} i \frac{\partial^2 \omega}{\partial s \partial \bar{s}} \quad (3.25g)$$

In conclusion the vorticity equation in its complex field form is:

$$\frac{\partial \omega}{\partial t} + V \frac{\partial \omega}{\partial s} + \bar{V} \frac{\partial \omega}{\partial \bar{s}} = \frac{4}{R_e} \frac{\partial^2 \omega}{\partial s \partial \bar{s}} \quad (3.26a)$$

which is exactly analogous to

$$\frac{\partial \omega}{\partial t} + (V \cdot \nabla) \omega = \frac{1}{R_e} \Delta \omega \quad (3.26b)$$

or

$$\frac{d\omega}{dt} = \frac{1}{R_e} \Delta \omega \quad (3.26c)$$

which is the basis of Lagrangian particle methods. It means that if the vorticity is confined to a point, and if this point is followed in its motion, the vorticity will not change.

Defining the equivalent Poisson brackets as:

$$[\omega, \psi] = -2i \frac{\partial \psi}{\partial \bar{s}} \frac{\partial \omega}{\partial s} + 2i \frac{\partial \psi}{\partial s} \frac{\partial \omega}{\partial \bar{s}} \quad (3.27)$$

then the vorticity equation can be written as

$$\frac{\partial \omega}{\partial t} + [\omega, \psi] = \frac{4}{R_e} \frac{\partial^2 \omega}{\partial s \partial \bar{s}} \quad (3.28)$$

Suitable “stand alone” forms of the streamfunction can be found by looking for solution of the degenerated case where the  $R_e$  parameter is very high. In this case solutions in the form of radial functions for instance can be looked after:

$$\psi(s, \bar{s}, t) = g(s\bar{s}, t) \quad (3.29)$$

Thus

$$\frac{\partial \psi}{\partial \bar{s}} = sg', \quad \frac{\partial \psi}{\partial s} = \bar{s}g' \quad (3.30)$$

and

$$\omega = -4 \frac{\partial}{\partial s} (sg') = -4(g' + s\bar{s}g'') \quad (3.31)$$

So the vorticity is also a radial function

Therefore

$$\frac{\partial \omega}{\partial s} = -4 \frac{\partial (g' + s\bar{s}g'')}{\partial s} = -4(2\bar{s}g'' + s\bar{s}^2 g''') \quad (3.32a)$$

$$\frac{\partial \omega}{\partial \bar{s}} = -4 \frac{\partial (g' + s\bar{s}g'')}{\partial \bar{s}} = -4(2sg'' + s^2 \bar{s} g''') \quad (3.32b)$$

Therefore the Poisson bracket's gives

$$[\omega, \psi] = -2i \frac{\partial \psi}{\partial \bar{s}} \frac{\partial \omega}{\partial s} + 2i \frac{\partial \psi}{\partial s} \frac{\partial \omega}{\partial \bar{s}} \quad (3.33a)$$

$$[\omega, \psi] = -2i \left( \frac{\partial \psi}{\partial \bar{s}} \frac{\partial \omega}{\partial s} - \frac{\partial \psi}{\partial s} \frac{\partial \omega}{\partial \bar{s}} \right) \quad (3.33b)$$

$$[\omega, \psi] = -2i \left( \begin{array}{l} sg'(-4)(2\bar{s}g'' + s\bar{s}^2 g''') \\ + \bar{s}g'4(2sg'' + s^2 \bar{s} g''') \end{array} \right) \quad (3.33c)$$

$$[\omega, \psi] = 8i \left( \begin{array}{l} sg'(2\bar{s}g'' + s\bar{s}^2 g''') \\ - \bar{s}g'(2sg'' + s^2 \bar{s} g''') \end{array} \right) \quad (3.33d)$$

$$[\omega, \psi] = 8ig'(2s\bar{s}g'' + s^2 \bar{s}^2 g''') - 2s\bar{s}g'' - s^2 \bar{s}^2 g''') \quad (3.33e)$$

$$[\omega, \psi] = 0 \quad (3.33f)$$

Therefore, any radial function for the streamfunction is a “stand alone” solution of the reduced vorticity equation (without boundaries and no

asymptotic velocity). All previous examples (Rankine, Oseen, etc...) possess this kind of radial symmetry.

Now if we consider

$$\psi(s, \bar{s}, t) \equiv -\frac{\Gamma_V}{4\pi} \left( \log(|s - s_V|^2) + E_1 \left( \beta \frac{|s - s_V|^2}{r_C(t)^2} \right) \right), \quad (3.34)$$

with  $r_C(t) = \sqrt{\frac{4}{R_e} \beta t + cte}$ , it is easy to prove from above that this is a solution to the viscous Navier Stokes equations in the case of incompressible flow without boundaries and no velocity at infinity

### 3.1.4. Bernoulli equations

Looking at the special case of an ideal fluid (irrotational, inviscid and incompressible), from the vorticity equation it can be deduced that

$$\frac{\partial V}{\partial s} = 0 \Rightarrow \frac{\partial \bar{V}}{\partial s} = \frac{\partial \bar{V}}{\partial \bar{s}} = 0 \Rightarrow \bar{V} \frac{\partial V}{\partial s} = \frac{\partial}{\partial s} (|V|^2) \quad (3.35)$$

and using the complex potential function  $F$  defined as

$$\begin{cases} \varphi = \frac{F(s) + \bar{F}(\bar{s})}{2} \\ \psi = \frac{F(s) - \bar{F}(\bar{s})}{2i} \end{cases} \quad (3.36)$$

where  $\varphi$  is the potential and  $\psi$  the streamfunction, we notice that

$$\begin{cases} V(\bar{s}) = \text{grad}(\varphi) = 2 \frac{\partial \varphi}{\partial s} \\ V(\bar{s}) = -2i \frac{\partial \psi}{\partial s} \end{cases} \quad (3.37)$$

and so the unsteady term can be written as:

$$\frac{\partial V}{\partial t} = \frac{\partial(2\partial\varphi/\partial t)}{\partial s} \quad (3.38)$$

Thus we can write:

$$2 \frac{\partial \varphi}{\partial t} + \bar{V}V = -2p + C(s, t) \quad (3.39)$$

and as every term of this equation should be real

$$\overline{C(s, t)} = C(s, t) = G(\bar{s}, t), \quad (3.40)$$

thus:

$$C(s, t) = f(t) \quad (3.41)$$

$$\frac{\partial \phi}{\partial t} + \frac{\bar{V}V}{2} + p = C(t) \quad (3.42)$$

which is exactly the unsteady Bernoulli equation for an ideal fluid. Therefore, if an analytical expression is found for the potential, the velocity field, the pressure and thus the forces experienced by the blade are known analytically.

### 3.1.5. Strategy of solution for the multibody problems

The main idea developed in the present thesis is to avoid computationally intensive methods involving matrix reversion and meshes by using various descriptions of different areas in the flow and including as much as possible analytical solutions inherited from early aerodynamic pioneers: Joukowsky [45], Theodorsen [46] and later on Couchet [47]. The method applied here benefits from a general conformal mapping transform (see Paper I) that allows the conversion of any set of sections into a set of circles. This allows coupling the strength of the analytical solutions with modern methods to handle the  $N$ -body problem of vortex-to-vortex interactions occurring in complex wake effects as in H-rotors.

Another numerical method, the panel method, can also be used to compute fast complex ideal flows around arbitrary airfoils without requiring conformal mapping transformation. However, as shown in Paper I, the panel method is slower and less accurate than the methods developed here.

It is assumed that high Reynolds number flows (more than 100 000) with wakes from airfoils at low angle of attack ( $<15^\circ$ ) can be correctly modeled by ideal flows with point vortices using Lamb Oseen or Rankine vortices only as regularization functions when vortices are close to each other. For this case a wide range of exact solutions exists for circular geometries.

The present simulation method has been built on the following steps

- i Create an algorithm which can transform any set of sections into a set of circles and vice et versa (paper I)
- ii Derive an analytic solution for a single section in arbitrary motion and varying input flow field both in terms of flow and in terms of forces experienced by the section (paper II)
- iii Model H-rotor flow: derive a semi analytic solution for the case of  $N$  sections in H-rotor motion (paper III)
- iv Model special load cases and aeroelasticity: generalize the single analytic arbitrary motion solution to the case of  $N$  blade H-rotor flows (paper IV)

## 3.2 Geometry– boundary conditions

In the following, turbines will only be considered along a horizontal section. In addition to the rotor geometry defined in 2.2, the section of the blade is defined with the parameters described in Fig 13 below.

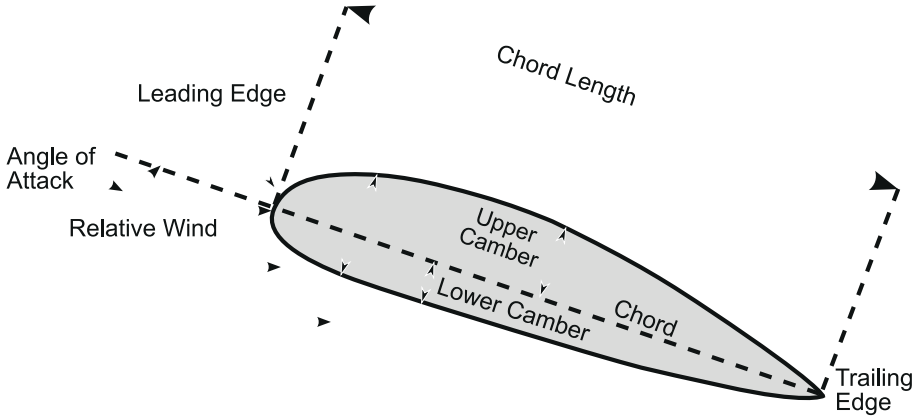


Figure 13. Description of airfoil section design parameters [48]

The airfoil coordinates are given by a set of discrete coordinates  $(x_{Ci}, y_{Ci})$  converted into a set of complex numbers  $z_{Ci} = x_{Ci} + iy_{Ci}$ .

In the special instance of the vertical axis turbine, the four key position parameters described in Fig 8 are:

- the rotor radius  $a(t)$ ,
- the pitch angle  $\delta(t)$ ,
- the blade shift position  $x_0(t)$
- the angular position of the blade at time  $t$ ,  $\beta(t)$

These four parameters are allowed to change arbitrarily with time. Additionally in the coordinate system  $z$ , three coordinate systems  $z_1$ ,  $z_2$ ,  $z_3$  are defined as follows:

$$z_1 = (z + x_0)e^{-i\delta}, \quad (3.43)$$

$$z_2 = z_1 + ia, \quad (3.44)$$

$$z_3 = z_2e^{i\beta}, \quad (3.45)$$

which represent rigid displacement and rigid rotations of the foil.

The  $z$  coordinates represents the position of the points fixed to the foil and the coordinates  $z_3$  the points seen by an observer fixed on the earth frame and looking to the turbine from above. A point attached to the  $z$  frame is moving in the  $z_3$  frame with the velocity

$$V_{z/z_3inz_3} = i\dot{\beta}z_3 + \dot{x}_0e^{-i(\delta-\beta)} - i\dot{\delta}z_1e^{i\beta} + i\dot{a}e^{i\beta} \quad (3.46)$$

expressed in the  $z_3$  frame coordinates. This is denoted in Eq 3.46 with the subscript  $z/z_3inz_3$ .

Under the assumption of incompressible and inviscid flow in the (assumed) inertial earth frame (or the lab frame), we obtain for the velocity  $V_3$  in this  $z_3$ -inertial frame:

$$\vec{\nabla} \cdot \vec{V}_3 = 0, \quad (3.47)$$

and adding the extra condition of irrotational flow in the lab :

$$\vec{\nabla} \times \vec{V}_3 = 0. \quad (3.48)$$

Thus we introduce two potential functions  $\varphi$  and  $\psi$  which respectively are the velocity potential and the stream function, satisfying Laplace's equation and the Cauchy-Riemann relations [45]. A complex potential is introduced for this ideal flow  $F = \varphi + i\psi$ , such that

$$V_3 = \overline{\frac{dF}{dz_3}}, \quad (3.49)$$

where the bar symbol represents complex conjugate. Any function  $F$  which is an analytic function is a solution to Eq 3.47 and 3.48 which are degenerated forms of Eq 3.4g and 3.6f.



This problem is subjected to three boundary conditions. A first boundary condition states that the velocity should coincide with the wind velocity at infinity. A second boundary condition states that the fluid should not penetrate inside the wing in the non-inertial  $z$  frame. An extra boundary condition analog to the Kutta-Joukowski condition will be introduced by stating that the velocity in the non inertial frame should be exactly zero at the trailing edge.

The conformal transformation  $f$  is considered in the form of a Laurent series

$$z = f(s) = s + \sigma_0 + \sum_{k=1}^{+\infty} \frac{c_k}{s^k} b^k, \quad (3.50)$$

where  $\sigma$  and  $c_k$  are complex numbers. The function  $f$  transforms a circle  $s_c$  of radius  $b$  in the  $s$ -plane into the wing section  $z_\alpha$  in the  $z$ -plane, represented by a discrete set of points.

$$s_c = b e^{i(\eta + \eta_{TE})}, \quad (3.51)$$

where  $\eta_{TE}$  is the trailing edge angle in the transformed plane. The way of finding the conformal mapping parameters for any airfoil shape and H-rotor sections will be explained in the next section.

Hence a complex potential which is an analytical function and fulfills the following three boundary conditions:

$$\frac{dF}{ds} \xrightarrow{s \rightarrow \infty} V_0 e^{i(-\alpha + \beta - \delta)}, \quad (3.52a)$$

$$F(s) - \bar{F}(\bar{s}) - 2i\psi_3(s, \bar{s}) = iK, \text{ for } s\bar{s} = b^2, \quad (3.52b)$$

$$\frac{dF}{dz_3} - \bar{V}_{z/z_3} = 0 \text{ for } s = b e^{i\eta_{TE}}. \quad (3.52c)$$

is a solution to the problem. In Eq 3.52a,  $V_0$  is the norm of the wind speed and  $\alpha$  is the angle between the wind velocity and the real axis. Eq 3.52b is expressed for all points in a circle that are mapped to the foil.  $K$  is real valued and the stream function  $\psi_3$  is representing the blade in vertical axis motion by

$$\psi_3(s, \bar{s}) = -\frac{1}{2} \dot{\beta} z_3 \bar{z}_3 + \frac{1}{2} \dot{\alpha} z_1 \bar{z}_1 + \text{Im}(-i\dot{\alpha} z_1 + \dot{x}_0 z) \quad (3.53)$$

Note that the flow represented by  $\psi_3$  is not an irrotational flow as according to Eq 3.6e.

$$\Delta \psi_3 = 4 \frac{\partial^2 \psi_3}{\partial z_3 \partial \bar{z}_3} = -\omega_3 \neq 0 \quad (3.54)$$

### 3.3 Conformal mapping

For a full review of conformal mapping method and technique used here see Paper I.

A conformal mapping is a transformation from the complex plane into the complex plane, which preserves the local angles. Riemann [49] showed that there exists one unique conformal map, which transforms the exterior of any shape (here a single airfoil) into the exterior of the unit disk. In the case of  $N_w$  wing sections, the existence of the mapping transformation is given by the Koebe theorem [50]: Every n-ply connected region can be conformally mapped into an exterior region that is bounded by n circles.

In the past, such transformations have been extensively used to provide exact solutions of Laplace's equation with Dirichlet type boundary conditions.

In aerodynamics, Laplace equation arises when the flow is assumed irrotational and incompressible. The Laplace equation and more generally the constant curl Laplacian [51] also arises in problems involving multiple bodies in motion with vortices.

The conformal mapping transformation is analytic. Therefore the transform has a Laurent series expansion. One of the goals of paper I is to describe a numerical method to find the transform of one circle into a given wing profile and  $N_w$  circles into  $N_w$  given wing profiles. The advantages of using Laurent's series representation are that it allows fast computation to the desired degree of accuracy.

#### Single section mapping

The airfoil coordinates for a single wing are given by a set of discrete coordinates  $(x_\alpha, y_\alpha)$  converted into a set of complex numbers  $z_\alpha$ . A conformal transformation  $f$  in the form of Laurent' series is:

$$z = f(s) = s + \sigma_0 + \sum_{k=1}^N \frac{c_k b^k}{s^k}, \quad (3.55a)$$

The serie in Eq 3.55a is convergent on and outside the circle boundary  $s_c$ . The aim is to find the optimal  $\sigma_0$  and  $\{c_k\}_{k \in \mathbb{N}}$ , which approach as closely as possible the shape given by interpolation of the points  $z_i$  of the airfoil section. This method is described in Paper I and can be applied to very wide section types including fatback sections with sharp angles.

#### Multiple section mapping

The transform, for the multicomponent section, the transform from  $N_w$  circles into  $N_w$  given wing profiles will be derived as:

$$z = g(s) = s + \sum_{n=1}^{N_w} \sum_{k=1}^N \frac{c_{n,k} b_n^k}{(s - s_{center,n})^k}, \quad (3.55b)$$

where  $N_w$  is the number of wings, and  $\{c_{n,k}\}_{k \in N, n \in N}$  are complex numbers. The function  $g$  transforms  $N_w$  circles  $s_{c,n}$  in the  $s$ -plane into  $N_w$  wing sections  $z_{\alpha,n}$  in the  $z$ -plane, represented by a given set of discrete points.

$$s_{c,n} = s_{center,n} + b_n e^{i(\eta + \eta_{TE,n})}, \quad (3.56)$$

$$z_{\alpha,n} = g(s_{c,n}), \quad (3.57)$$

where  $b_n$  is the radius of the  $n$ th circle in the  $s$  plane,  $s_{center,n}$  its center and  $\eta_{TE,n}$  is the angle representing the trailing edge.

### H-rotor section mapping

In particular for a periodic problem, assuming that the  $n$ th blade is obtained from the first blade by a rotation of  $n\Delta\beta$ , the  $g$  transform can be simplified into

$$z = g(s) = s + \sum_{n=1}^{N_w} \sum_{k=1}^N \exp[i(n-1)(k+1)\Delta\beta] \frac{c_{1,k} b_1^k}{(s - s_{center,1} \exp(i(n-1)\Delta\beta))^k} \quad (3.58)$$

and the  $N_w$  circles representing the  $N_w$  wings will be defined as

$$s_{c,n} = s_{center,1} \exp[i(n-1)\Delta\beta] + b_1 e^{i[\eta + \eta_{TE,1} + (n-1)\Delta\beta]}, \quad (3.59)$$

$$z_{c,n} = g(s_{c,n}). \quad (3.60)$$

In other words, when the system is periodic, only the coefficients for the first wing need to be established to produce the full section.

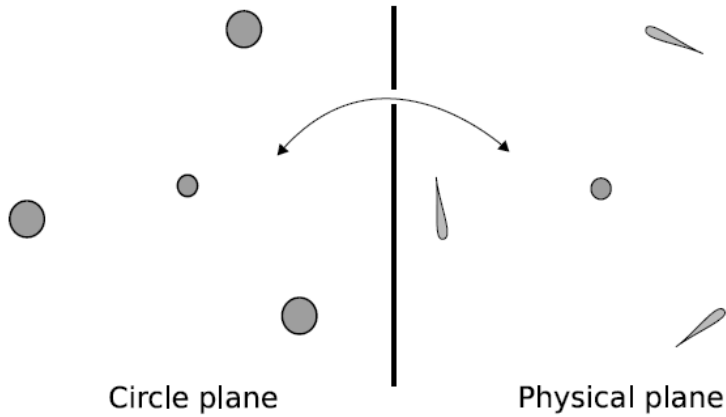


Figure 14. Transform of the physical plane to the circle plane and vice versa through a conform mapping

Various examples of the abilities of the method are presented in Paper I. The method has been shown to transform fast and accurately any type of 2D sections and sets of sections especially for H-rotor.

### 3.4 Analytical solutions

#### 3.4.1. Solution of the single blade problem with vortices

Regarding the form of Eq 3.52a, 3.52b and 3.52c, it seems appropriate to look for a transform  $F(s)$  in the form of an analytic function (which automatically verifies potential flow equations) and express it in the form of a Laurent's series similarly to the airfoil transform. Thus, considering the asymptotic behavior of  $F$  at infinity up to a constant:

$$F(s) = V_0 e^{i(-\alpha+\beta-\delta)} s + V_0 e^{-i(-\alpha+\beta-\delta)} \frac{b^2}{s} + \sum_{v=1}^{N_v} \left[ \frac{i\Gamma_v}{2\pi} \left( \log(s - s_v) - \log\left(s - \frac{b^2}{\bar{s}_v}\right) \right) \right] + F_1(s) \quad (3.61a)$$

where  $\Gamma_v$  are the strengths of the wake vortices and their images. These  $\Gamma_v$  are primarily a consequence of the unsteady motion of the wing (technically the Kutta condition at the trailing edge). At each step one trailing vortex with

a given strength is created and then shed. The set of these trailing vortices forms the wake of the foil and when combined the wake of the turbine.

The function  $F_1$  is given as

$$F_1 = \sum_{k=1}^{\infty} \frac{G_k}{s^k} b^k, \quad (3.61b)$$

where

$$G_k = -i\dot{\beta}G_{A,k} + i\dot{\delta}G_{B,k} - i\dot{a}G_{C,k} + \dot{x}_0 G_{D,k}. \quad (3.62)$$

All coefficients  $\{G_k\}_{k \geq 1}$  can be derived analytically by straightforward identifications from the non-penetration boundary condition in Eq. 3.52b. The coefficients can be found in Appendix A of Paper I. The complex potential  $F$  is now totally determined and corresponds to the exact solution of Laplace's equation for an arbitrary boundary in arbitrary two dimensional motion. The streamlines in the  $z$  plane can be found by determining the isovalues of the function

$$\psi_r = \text{Im}(F) - \psi_3. \quad (3.63)$$

### 3.4.2. Velocity field

Knowing the complex potential  $F$ , the “absolute” velocity is derived in the  $z$ -plane as

$$V_z = \frac{\overline{dF}}{dz} = \frac{\overline{dF}}{ds} \frac{ds}{dz}, \quad (3.64)$$

and the absolute velocity in the  $z_3$  frame is derived as

$$V_3 = \frac{\overline{dF}}{dz_3} = V_z \frac{dz}{dz_3}. \quad (3.65)$$

The relative velocity expressed in the  $z_3$  frame for a point fixed to the foil (attached to the  $z$  frame) is then

$$V_{R3} = V_3 - V_{z/z_3 \text{ in } z_3}. \quad (3.66)$$

### 3.4.3. Kutta condition

The Kutta condition is satisfied at each time step by locating a new vortex at the trailing edge of the profile in the way described by Streitlien [52]. The strength of this vortex is determined using the Kutta Joukowski condition described in Eq 3.67a.

$$\frac{dF}{dz_3} - \bar{V}_{z/z_3 \text{ in } z_3} = 0, \quad (3.67a)$$

at the trailing edge point  $s = be^{i\eta_{TE}}$ .

Assuming that  $N_V - 1$  vortices are present in the flow from the  $N_V - 1$  previous time steps, let  $s_{N_V}$  be the position of the newly emitted vortex in the  $s$  plane and  $s_{TE}$  the position of the trailing edge. It is now possible to determine the unknown nascent circulation by

$$\left. \frac{dF}{ds} \right|_{s_{TE}} = \bar{V} \left. \frac{dz}{ds} \right|_{s_{TE}}. \quad (3.67b)$$

### 3.4.4. Numerical implementation

All the created vortices are advanced in time according to the absolute velocity of the fluid. At each vortex location the convection velocity is corrected using Routh's rule [53]. The update of the vortex positions in the circle plane can be carried out following the direct procedure of Paper III or the developed inverse mapping procedure developed in Paper I. Under the inviscid assumption the strength of all vortices is kept constant (see Eq 3.26c) once they are ejected. The vortices are modeled as points built up on Rankine kernels (Eq 3.8) or Lamb Oseen (Eq 3.12) when necessary. The computationally expensive convection of the vortices is carried out using the Fast Multipole Method (see Paper II) when possible and the images are automatically taken care via a developed fast imaging method (see Paper I).

### 3.4.5. Forces evaluation

The elemental force due to the pressure from the fluid on the blade can be evaluated via the complex number

$$dF = ipdz. \quad (3.68a)$$

The inviscid pressure forces can be integrated numerically and are given in the  $z$  frame by

$$X - iY = -\oint_C ip\bar{z}dz, \quad (3.68b)$$

where  $C$  is the airfoil contour in the  $z$  plane. The pitching moment with respect to the origin of the  $z$  plane is

$$M_0 = \text{Re} \left[ \oint_C pz\bar{z}dz \right]. \quad (3.69)$$

In the present work the final analytical formulas for the pitching moment calculations are not presented. However, with the use of the extended Blasius formula [54] and the residue theorem the analytical calculation can be carried out [52]. The forces can be integrated analytically (for details see Paper II). It is found that

$$X - iY = \frac{i\rho}{2} [E + I], \quad (3.70a)$$

with

$$\begin{aligned}
E = & -2\left(2(\dot{\beta} - \dot{\delta})\pi\left(V_0 e^{i(-\alpha+\beta-\delta)} b^2 + \bar{G}_1 b - V_0 e^{-i(-\alpha+\beta-\delta)} \bar{c}_1 b\right)\right. \\
& - 2(\dot{\beta} - \dot{\delta})\bar{V}_{z/z3inz0} A + i(\dot{\beta} - \dot{\delta})^2 \frac{4A}{3} \bar{\zeta} - \frac{4A}{3} \bar{\zeta} [\dot{\delta} - \dot{\beta}] - 2iAA_{z/z3inz} \left. \right), \quad (3.70b) \\
& + 4i\pi b \left( \bar{c}_1 \left[ \frac{\partial V_0}{\partial t} e^{-i(-\alpha+\beta-\delta)} - V_0 i(-\dot{\alpha} + \dot{\beta} - \dot{\delta}) e^{-i(-\alpha+\beta-\delta)} \right] - \bar{D}_1 \right)
\end{aligned}$$

where  $A_P$  is the area of the profile,  $\zeta$  the complex position of the center of moment and  $V_{z/z3inz0}$ ,  $A_{z/z3inz}$  and  $D_1$  are given in Appendix B of paper II.

$$\begin{aligned}
I = & 2 \sum_{v=1}^{N_v} \Gamma_v \frac{d\bar{z}_v}{dt} - 2\bar{V}_{entz0} \sum_{v=1}^{N_v} \Gamma_v + 2i(\dot{\beta} - \dot{\delta}) \sum_{v=1}^{N_v} \Gamma_v \left[ \bar{z}_v - \bar{s}_v + \frac{b^2}{s_v} \right], \quad (3.70c) \\
& - 2 \sum_{v=1}^{N_v} \Gamma_v \left( \frac{\partial \bar{s}_v}{\partial t} \frac{d\bar{z}_v}{ds_v} - \frac{\partial \bar{s}_v}{\partial t} + \frac{\partial}{\partial t} \left( \frac{b^2}{s_v} \right) \right)
\end{aligned}$$

To include the nascent vortices this last formula is rephrased as

$$I \cong -2i(\dot{\beta} - \dot{\delta}) \sum_{v=1}^{N_v} \Gamma_v \left[ \bar{s}_v - \frac{b^2}{s_v} \right] + 2 \frac{\partial}{\partial t} \left[ \sum_{v=1}^{N_v} \Gamma_v \left( \bar{s}_v - \frac{b^2}{s_v} \right) \right]. \quad (3.70d)$$

The formula in 3.70d is straight forward to implement numerically. The last term can be evaluated numerically by a finite difference scheme. For H rotor computations a third order scheme will lead to stable computation whereas a second order scheme will be stable for pitching computation. The first order scheme is unstable for any simulations including rotations.

### 3.4.6. Synthesis of the single blade analytical solution

The analytical solution of the problem (Eq 3.47, 3.48, 3.52a, 3.52b and 3.52c) is known and described with its numerical implementation in Paper I and II. The main process to find all outputs of interest is for the single wing problem:

1. Calculation of the coefficients in the Laurent's series describing the complex velocity potential from the input parameters and their history
2. Creation of a new vortex emitted into the flow field close to the trailing edge of the wing to fulfill the unsteady Kutta condition
3. Calculations of the loads on the blades by numerical integration of the pressure or using Eq 3.70d described in Paper II.
4. Stepping the position of the vortices in time through the fast imaging procedure (Paper I) and the FMM procedure (Paper II) and going back to step 1.

### 3.4.7. Multiblade solution

The above procedure has been explained for a single blade turbine. In Paper III, it is showed possible to generalize this to an analytical solution of the  $N_W$  section problem. The conformal mapping of  $N_W$  sections is used as described in Paper I. Thus, this method is valid for turbines with no motion of the sections with respect to the others: the full  $N_W$  blade section is considered as a rigid body in rotation. Therefore Paper III study assumes non-pitching and non-translating blades. However for a wide range of studies: performance assessment, wake characterization, loads for rigid blades, the model of Paper III is accurate enough. However the method can not be adapted for an aeroelastic coupling to study the effect of the small motions of sections in the plane.

The generalization of paper II to take into account the desired unsteady effects without having to use a full conformal mapping procedure at each step is described in paper IV. It uses exactly the same routine as in § F treating the  $N_W$  wing sections independently. This means that each of the  $N_W$  section is experiencing all vortices present in the flow and particularly the ones emitted from all other wings.

In particular at each time steps, the effect of one wing on the other is only seen through the action of its vortices (see Fig 15). The procedure is repeated for each wing.

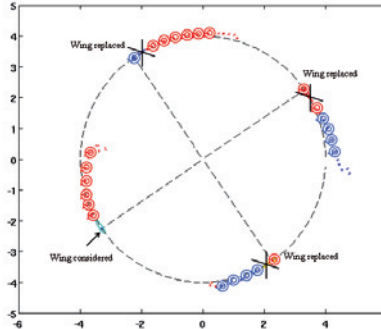


Figure 15. Principle for multi blade generalization from single blade analytic solution

When one wing is considered, all other sections are erased (see Fig 15). However it is appropriate to place one vortex at the quarter chord of the erased wings with its intensity equal to the sum of all vortices which were found inside the section when the wing was treated at the previous time step. All vortices except the quarter chord ones are stepped in time.

With this procedure and after some time steps all wings are seeing different vortices positions due to the small errors that are added at each time step. To correct this effect, all vortices are averaged at some defined time steps.



However this generalization, which is an approximation gives for turbines with solidity less than 1, accurate results compared to the procedure of Paper III. The results of this generalization have been carefully validated in Paper III in terms of vortices position and normal and tangential forces.

In conclusion for the generalization of Paper II results for a single blade into a multi blade solution, Paper III procedure is faster as it solves the problem of  $N_W$  rigid wings once (the vortices are stepped only once) and paper IV method solves  $N_W$  problem for  $N_W$  sections. However, Paper III model would need extensions to be able to treat independent motions of each blade section, which is required for the coupled aero-elastic mode whereas this is straightforward in Paper IV version.

### 3.5 Aeroelasticity

The main aim of paper IV is to couple aerodynamics and elastics for vertical turbines. This is achieved by using the described generalization and assuming that there is no interaction between horizontal planes in the aerodynamic domain. Instead this interaction occurs through the different kinematics of the sections given by the elastic model i.e. wings and supporting arms.

The supporting arms of the turbine are assumed free from any aerodynamic load. This assumption is not relying on any physical considerations but is made to build the present “first step” model.

The main inputs of the aerodynamic model (and inputs to the elastic modulus) are the position ( $Q$ ), the velocity ( $\dot{Q}$ ) and the acceleration ( $\ddot{Q}$ ) vectors of the section of wing studied in a horizontal plane plus the parameters representing the wakes induced by the wing. The main outputs of the model are the loads (forces and torques) felt by the different horizontal sections of each blade.

The elastic model is not described further here. The reader is referred to the full description given in Paper IV.

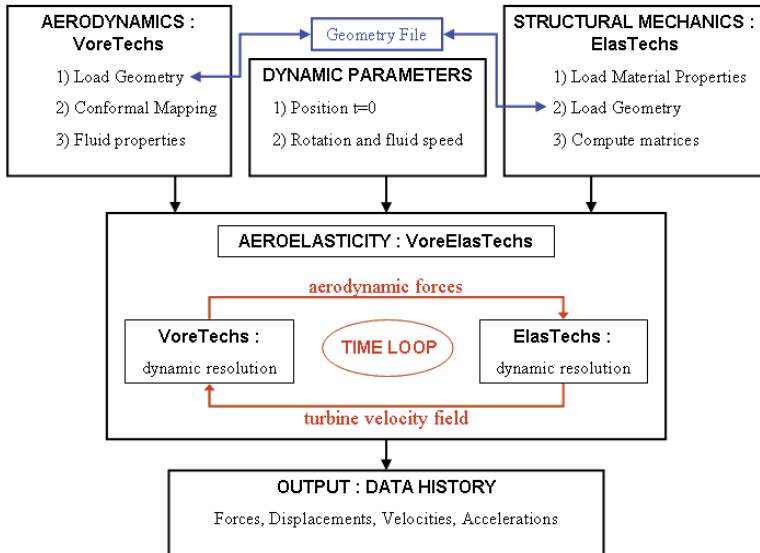


Figure 16. Computational structure of the aeroelastic model

### 3.6 Lower order models

All the models described in this section 3 deals with unsteady flows around an H-rotor under the main assumption that the flow is attached. Moreover 3D effects cannot be included.

To complete the simulation toolbox, the standard global double multiple streamtube model of Homicz [40] has been used and implemented into the Conformal mapping double multiple streamtube model (CMDMS code). The CMDMS code has been widely used for preliminary design studies for Papers V to VIII and MSc thesis [6].

The principle of the double multiple streamtube models is to divide the virtual flow going through the turbine into different streamtubes parallel to each other. Fig 17 shows an example of streamtube cut of an H-rotor section (the wind is blowing from the right on this figure). The streamtube model is referred to as a double one as the upwind part (half circle part of the horizontal rotor section in the right in Fig 17) and the downwind part (half circle part of the horizontal rotor section in the left in Fig 17) are treated sequentially as the blade passes through them each.

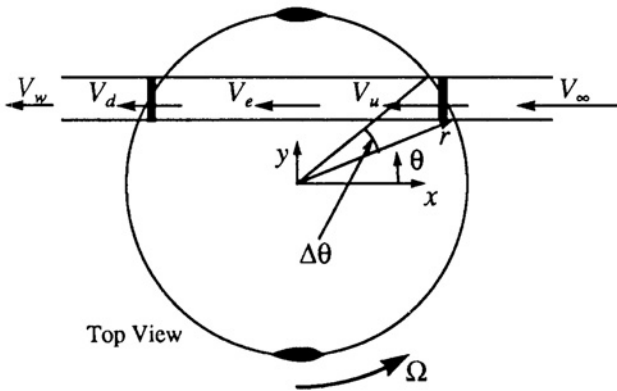


Figure 17. Streamtubes from above, wind coming from the right

The flow is further split in two parts: the overall flow part and the local flow part.

If enough streamtube are used, the wind in the vicinity of the upwind cut section can be assumed to be constant. The constant wind assumption can also be applied for the downwind section.

The equations giving the velocity and angles as well as the forces are solved for each streamtubes, and iterated to converge globally on the upwind and downwind path.

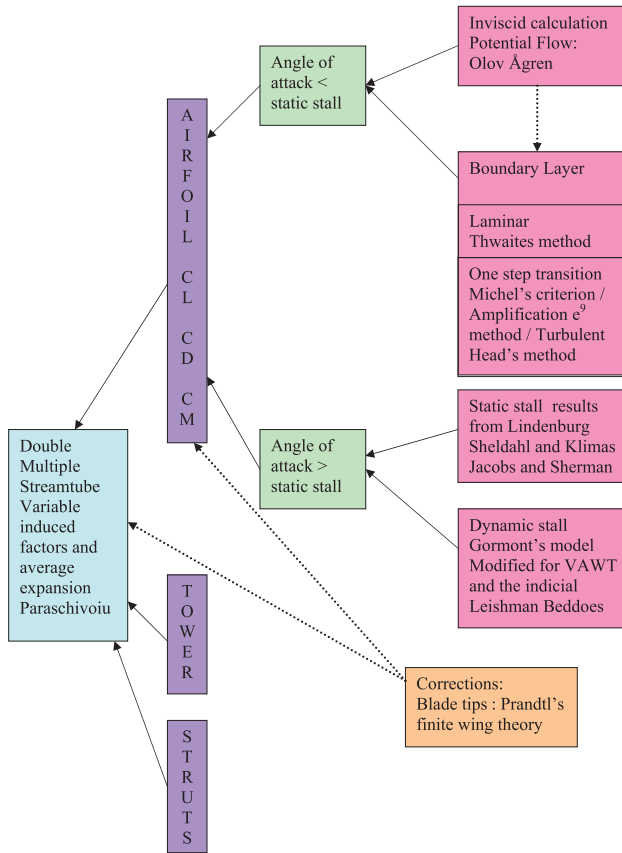


Figure 18. Simulation subsystems implemented into the CMDMS flow model

Within the streamtube formalism it is easy to include into the CMDMS model various corrections for

- a) Tip loss effects
- b) Dynamic stall effects
- c) Strut drag
- d) Horizontal flow expansion (flow expansion is naturally included in the vortex model of Paper II)
- e) Viscous effects on blades
- f) Vertical shear layer
- g) Tower shadow effects

In the CMDMS implementation, the analytic solution of Paper II is used in its steady rotating form to provide lift coefficients for low angles of attack. The local flow model is based on a conformal mapping of one blade section into a circle (see Paper I). Milne Thomson [54] showed that the flow of a circle rotating in an inviscid potential flow can be fully described

analytically. Wilson [55] applied it to the vertical axis case for a flat plate. The model used here is even more general and can represent any single blade section placed in an arbitrary external field (see Paper I). This analytical model provides the necessary input quasi static data in terms of lift and pitching moment via a quasi static form of Paper II theory.

To provide the necessary drag data, the inviscid velocity is used as input for a two equation laminar integral boundary layer method. The transition is predicted using the amplification  $e^N$  method and the turbulent layer is evaluated using Head's method [32]. The Drag data is then evaluated by the Squire-Young formula [56].

It may be noted that this integral boundary layer formulation was derived from the Polhausen equation [57] which is not valid for rotating flows. In the absence of modified integral methods for this peculiar problem, the method is still used to give an approximation which should be taken with caution [58]. However, the ordinary use of double multiple streamtube does not even take into account that the airfoil is rotating. Instead wind tunnel or numerical steady lift drag and pitching moment data are used. The present analytical procedure is particularly suited for a design procedure. It provides the local pressure distribution without requiring any extra computation time compared with the static data. In fact, only the boundary layer quantities (friction coefficients) require extra computation time.

The assumption of irrotational flow breaks down at low tip speed ratios due to the presence of dynamic stalling of the blades. The static coefficients from the flat plate experimental data are used as soon as the blade local angle of attack exceeds the static stall values. The dynamic stall model [59] is then used to simulate the encountered hysteresis loop.

The tangential forces can be assessed and the aerodynamic efficiency can be estimated once the process is iterated. The normal forces are calculated at each loop in the process.

This tool is the fastest of all tools developed in Paper I to IV. It is therefore very convenient to be used as a preliminary design tool giving an overall picture of the different design issues. The precise load cases to be further investigated can be detailed using the other more advanced models. However, it is important to remember that the CMDMS models and more generally streamtube models are quasi static and can not evaluate loads during start up of turbines or in the case of changing winds (directions or intensity) as well as aeroelasticity phenomenon. According to the author they can be used as global performance assessment tools but not detailed design tools.

## 4 Design studies

In the following paragraphs we will highlight the tests which have been performed to verify the various tools and simulation package developed in Chapter 3.

### 4.1 Comparison with benchmark cases

#### 4.1.1. Conformal mapping test case

The first implementation of the multicomponent mapping consists of a simulation of the Suddhoo-Hall [60] airfoil.

In terms of geometry, as for all smooth wing sections, a value of 64 terms in the Fourier expansions seems enough to provide a relative error of  $10^{-5}$  in the mapped shape. In the case of flat back airfoils, gurney flaps and spoilers, the number of terms needs to be increased.

To compare with the known exact pressure distribution, the pressure coefficient isolines around the full four element airfoil are obtained in Fig 19 by direct evaluation. The pressure coefficients are defined as:

$$C_{Pr} = \frac{p - p_{\infty}}{1/2\rho V_0^2}, \quad (4.1)$$

with  $\frac{p - p_{\infty}}{\rho} = -\frac{1}{2}(|V|^2 - |V_0|^2)$ , and thus  $C_p = 1 - |V|^2 / |V_0|^2$ .

The inviscid flow calculation given by the many circles flow is obtained by using 64 coefficients and evaluated on 1000 points on each airfoil.

The resulting accuracy is  $10^{-11}$  in terms of fulfillment of the boundary condition on all airfoil surfaces. The pressure coefficients, see Fig 20, are in very good agreement with the known analytical solution [60] which is not represented here as it cannot be distinguished from Paper I results on Figure 20.

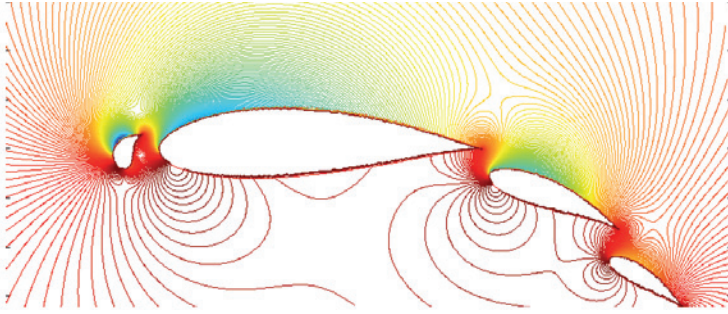


Figure 19. Sudhoo – Hall airfoil pressure coefficient computations

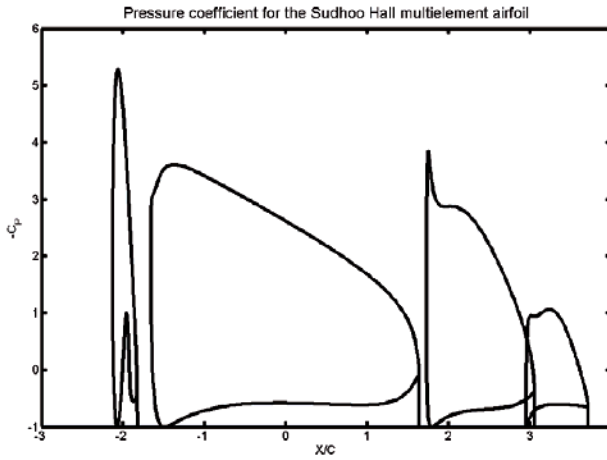


Figure 20. Sudhoo – Hall airfoil pressure coefficient computations as in Paper I

#### 4.1.2. Unsteady single blade test case

The second series of tests consider a single blade NACA0015 profile in unsteady sinusoidal pitch and heaving motion (which is important for aeroelastic coupling) at high Reynolds number of one million. The experimental data of Piziali [61] will be used. The simulation results from Paper I are tested against both experimental results from Piziali [61] and analytical formulas from Theodorsen [62]. The Theodorsen formulas model the unsteady behavior of a blade by modeling the wing as a flat plate. In these motions the main parameter to represent the unsteadiness is the reduced frequency

$$k = \omega_f c / 2V_0, \quad (4.2)$$

where  $\omega_f = 2\pi f$ ,  $f_r$  is the frequency of the pitching or heaving motion,  $c$  the airfoil chord and  $V_0$  the asymptotic wind speed i.e. forward translating speed of the foil.

The main numerical parameters such as the position of the nascent vortex, the kernel vortex type and the time step have small influence on the simulation results. The number of vortices at the end of each simulation (around 5 to 6 cycles) is in the range of 10 000. Due to the good computational efficiency of the Fast Multipole Method (FMM), the simulations require only a few minutes on a laptop 1.6 GHz personal computer.

The first benchmark case in Fig 21 considers a NACA0015 profile oscillating in pitch from 2 to 6 degrees with a reduced frequency of 0.038. The second benchmark case considers angle of attacks between 1.8 to 6.2 degrees at a reduced frequency of 0.19 (see Fig 22).

In Fig 21 the experimental results for the lift coefficients of Piziali [61] and the analytical results of Theodorsen [62] agree particularly well. The present simulation agrees for the qualitative behavior. However the simulated and experimental signals show a shift in the lift values. This behavior could be explained as Theodorsen [62] did not include all transients' effects. These effects underestimate the lift and nearly coincide with viscous effects. In the NASA experiments [61] the viscous effects would reduce the lift from the inviscid solution. The results of the simulation are therefore considered to be realistic within the approximations done within the model. In Fig 22 the same phenomenon is observed but the width of the hysteresis loop is decreased compared to the lower reduced frequencies. This appears to be correctly modeled by the present simulation. The present simulation shows the same shift to higher lift values compared to experimental results which is also due to the inviscid assumption. The underestimation in Theodorsen theory is obvious.



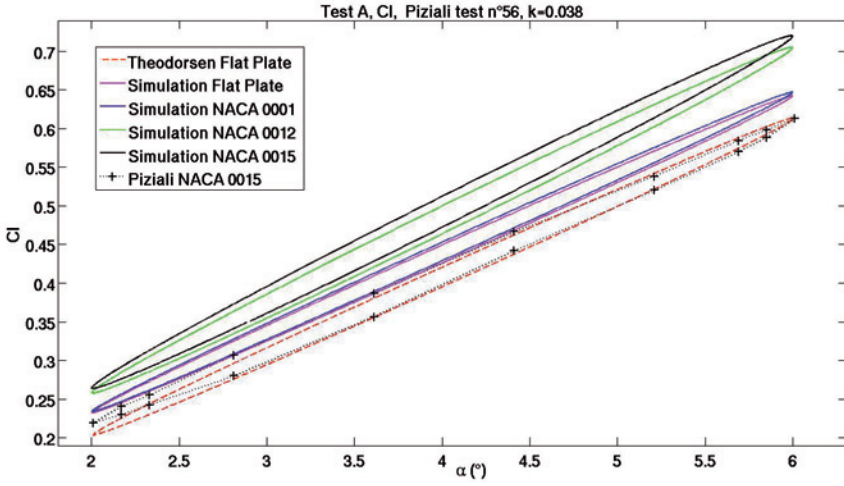


Figure 21. Lift coefficient vs. pitch angle for different profiles in sinusoidal pitching motion with a low reduced frequency of 0.038 from 2 to 6 degrees

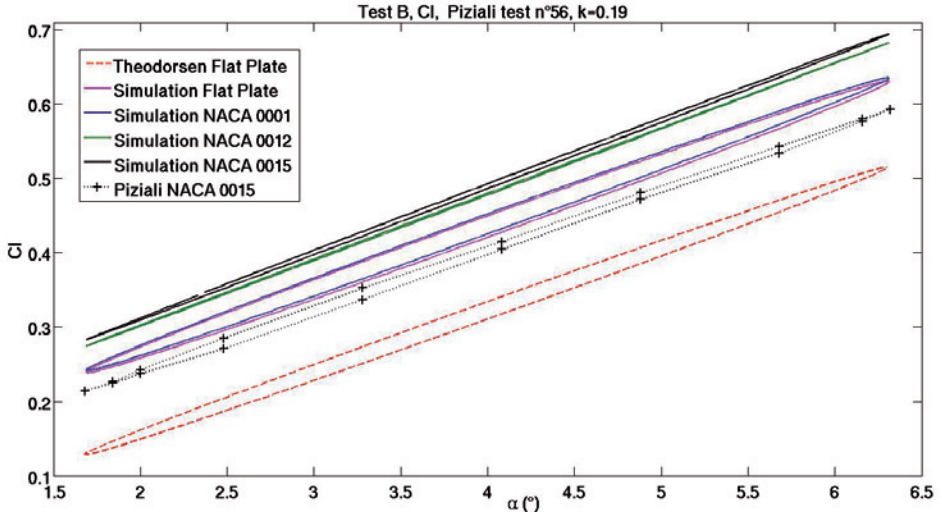


Figure 22. Lift coefficient vs. pitch angle for different profiles in sinusoidal pitching motion with a high reduced frequency of 0.19 with a pitch from 1.8 to 6.2 degrees.

## 4.2 VAWT measurement comparisons

### 4.2.1. Unsteady Normal and tangential forces

The normal and tangential force predictions on VAWTs, as well as the overall turbine efficiency, are key to ensure a good and robust design by correctly assessing loads. The tangential force is proportional to the torque coefficient produced by one blade (up to pitching moment corrections). The normal force coefficients are mainly important for fatigue issues on the carrying arms, junctions, and bending of the blades. They also contribute to the thrust force and lead to the tower and foundation dimensioning.

Only high TSR will be investigated here to test the accuracy of the vortex models developed in Paper II and III.

The simulation results are here directly compared with experimental wind tunnel results.

#### Single blade turbines

In all the following computations, a single bladed H rotor with a chord to radius ratio of 0.25 [34] (see Table 5) and operating at a tip speed ratio of 5 is considered.

Dimensional parameters	
Wing section	NACA0015
Chord	15,24 cm
Number of blades	1
Turbine radius	0.61m
Turbine height	1.1 m
Tip speed ratio	5
Blade Reynolds number	40 000
Attachment point	Mid chord
Pitch (positive as out)	0°
Non dimensional parameters	
Solidity	0.25
Chord to radius ratio	0.25
Aspect ratio	7.33

Table 4. Main parameters of the turbine described in [34]

In general the chord to radius ratio gives the effect of the curvature of the local flow. The aspect ratio gives the effect of the 3D effects and the solidity gives the optimum tip speed for the turbine. A turbine with high solidity will function at lower speeds than a low solidity turbine.

Concerning the numerical computation, each revolution of the rotor represents 200 to 400 time steps and the results are considered for the 6th revolution. The convection of vortices is carried out with direct summation for this low number of vortices and the time stepping scheme uses the

forward Euler method, as the Runge-Kutta method did not affect the results significantly. All computations lasted for 1-2 minutes on a 1.6 GHz laptop computer. This can be compared to hours of CPU time used in Ponta [51].

In Fig 23 the normal and tangential forces analogous to Oler [34] experimental and numerical study with one NACA0015 profile attached at the mid chord are plotted against the beta position. The non viscous simulation includes the unsteady motion of the blade plus one trailing vortex sheet whereas the viscous simulation also assumes one vortex sheet but includes in the drag calculations an integral boundary layer representation using a modified Thwaites' and Head's method [63]. This integral boundary layer representation has only been used for this test. It is similar to the one used in Oler [34] and applied to the same problem. The Reynolds number in Oler's experiments [34] is 40 000 and is outside the assumption of those theories but a qualitative agreement can be expected.

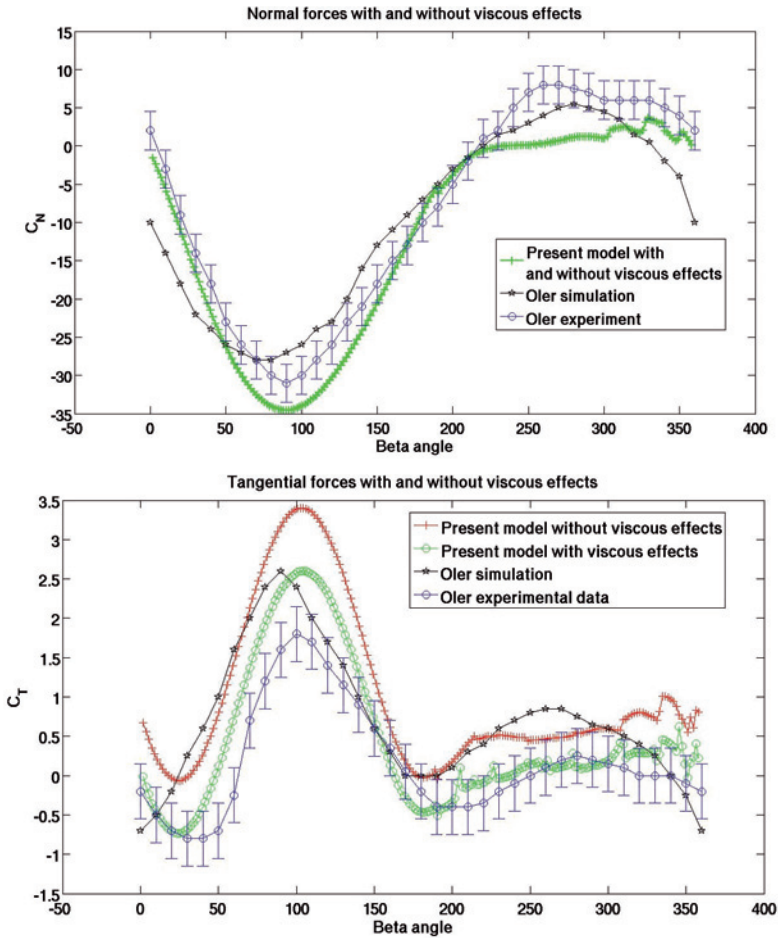


Figure 23. Normal and tangential force simulation versus experiment [34]

The viscous influence lowers the tangential force, as compared to the raw experimental data of Oler [34]. The results from the viscous and inviscid simulation qualitatively agree whereas the viscous simulation fits better (28% error in the tangential force coefficient in Fig 23 and 16% error for both simulations in the normal forces). The discrepancies between the viscous simulation and the experimental results for the normal force are first due to the low Reynolds number considered, which not only increases the drag but also significantly decreases the lift. Hence the power extracted from the upwind pass is too high and the speed is too much reduced in the downwind pass inducing simulated normal forces that are too low. Secondly, the aspect ratio used in Oler experiment [34] is low and might suggest a 3D influence. Other authors [51], [64] have not compared their simulation to this very hard case but instead compared with measurements of Klimas [65](see Table 6) with a two bladed H rotor at lower chord to radius ratio of 0.15. They found a general good agreement with their simulation. Generally, the results from other recent simulations [51], shows a similar agreement but at a much higher CPU time and the results of the vortex method in Fig. 23 of Oler [34] are poorer.

Dimensional parameters	
Wing section	NACA0012
Chord	9,14 cm
Number of blades	2
Turbine radius	0.61m
Turbine height	1.1 m
Tip speed ratio	5
Blade Reynolds number	40 000
Attachment point	Quarter chord
Pitch (positive as out)	0°
Non dimensional parameters	
Solidity	0.29
Chord to radius ratio	0.15
Aspect ratio	12

Table 5. Main parameters of the turbine described in [65]

The inviscid simulation is expected to provide a realistic model for higher Reynolds numbers. For instance, a typical Reynolds number value is about 300 000 for a kW range turbine.

## Multibladed turbines

In this section the experiment reported by Klimas [65] is considered; as the investigated H-rotor has two blades.

The results of the simulation using Paper III theory can be found in Fig 24. The agreement is fair for the normal force. There is a notable phase shift. This is thought to be an effect of neglecting the unsteady terms in the unsteady Bernoulli Eq 3.42 for computational speed optimization.

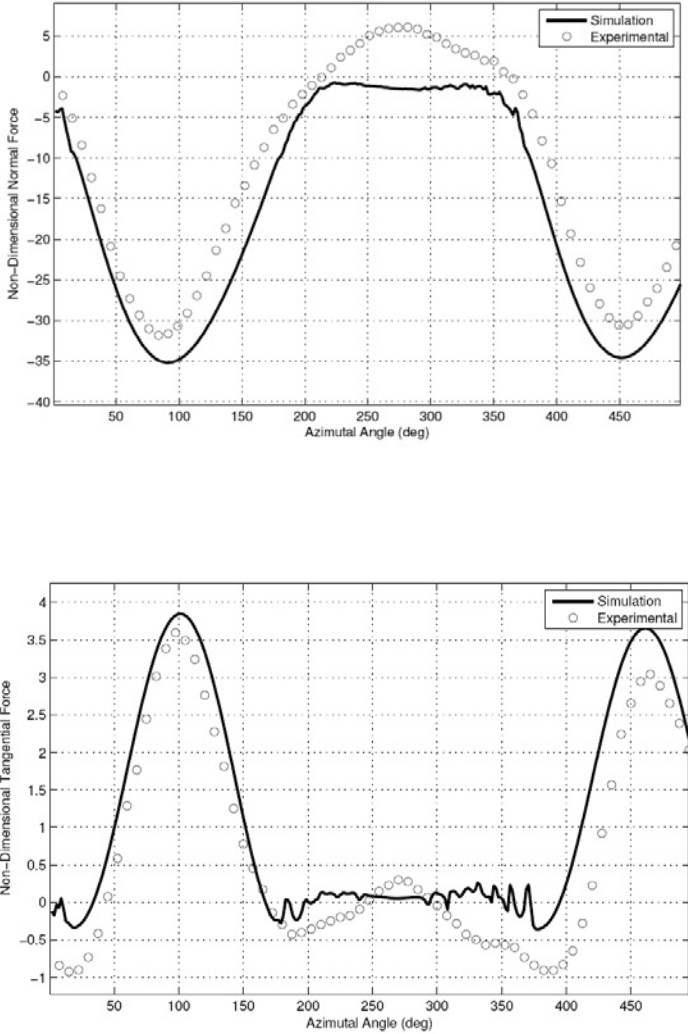
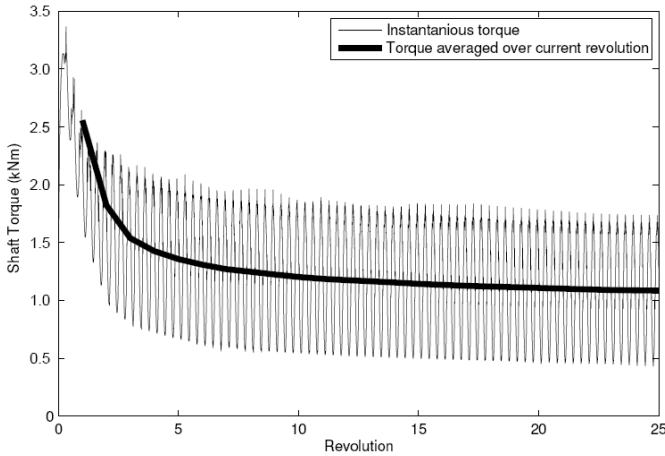


Figure 24. Normal and tangential forces on one of the blades of the turbine [65] after the third revolution

The good agreement in the tangential force is not suspect since it is the third revolution which is considered here rather than the asymptotic result. Therefore the simulated results should lead to an overestimate as the asymptotic behaviour is usually reached after around 10 revolutions.



*Figure 25.* Torque shaft unsteady behavior as a function for the 3 blade Marsta turbine described in Paper IV.

#### 4.2.2. $C_p$ curve comparisons

In terms of aerodynamic efficiency, CMDMS model are used as Vortex methods described here are able to assess only non separated flow from tip speed ratios higher than 4. The design calculations for the Marsta turbine (see paper VI) are compared with the measured results and later simulations [66].

Marsta turbine (paper VI) has the aerodynamic parameters given in Table 7.

Dimensional parameters	
Wing section	NACA0018
Chord	25 cm
Number of blades	3
Turbine radius	3 m
Turbine height	5 m
Tip speed ratio (design)	4
Pitch (positive as out)	0°
Attachment point	Quarter chord
Rated rotational speed	127 rpm
Maximum blade tip speed	40m/s
Rated wind speed	12 m/s
Rated power	12 kW
Strut section	NACA0025 (with flat back)
Non dimensional parameters	
Solidity	0.25
Chord to radius ratio	0.08
Aspect ratio	20

Table 6. Main parameters of the Marsta 12 kW turbine, Paper VI

### Design study first simulation results

The design simulation on the aerodynamic efficiency curve can be seen in red in Fig 26. It is important to note that when this paper was written, the CMDMS model was not including strut effects and that the strut airfoil sections had a flat back shape. The optimum tip speed ratio is found between 3.5 and 4 giving a maximum value of 40% of aerodynamic efficiency.

### Measurement and second simulation results

The measured results compared to the newly simulated results including strut corrections can be seen in Fig 26. The optimum tip speed ratio is found at 3.3 and giving a maximum value of 30% of aerodynamic efficiency whereas the new simulation result gives the right aerodynamic efficiency but shifted to higher tip speed ratio still around 4.

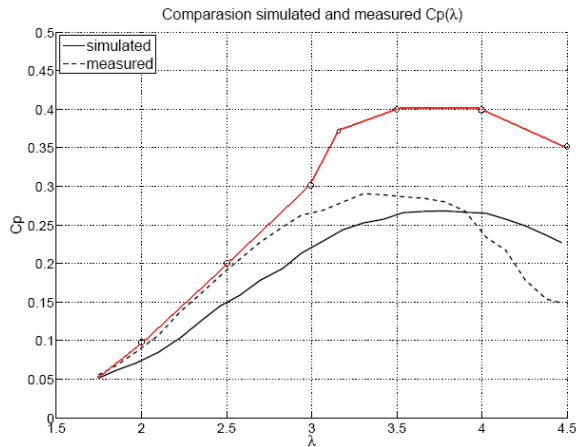


Figure 26. Comparison of design and measured power curve for Marsta turbine from Paper VI and [66]

Although the results of the first simulation and measured data significantly differ, the results are within a range which is acceptable considering the highly innovative concept considered. The key difference in the simulation models is included in the strut correction. The innovative strut design effect on the aerodynamics was not included well in the first design study.

The new simulations are in reasonable agreement with the measured peak value of the  $C_p$  curve. However, the values for both low and high tip speed ratios do not match as accurately. For low tip speed ratios, the effects of dynamic stall will be significant for the performance, and the accuracy of the dynamic stall model used [67] can be questioned for high angles of attack. Thus a mismatch between simulation and experiment could be expected for low tip speed ratios. For high tip speed ratios, the measured power coefficient decreases much faster than the simulated value for increasing tip speed ratio. However for high tip speed ratios, the maximum possible error estimation in the  $C_p$  curve is considerable.

#### 4.2.3. Wake studies

Although this comparison can be only made in a qualitative manner, as no precise wake analysis exists for vertical axis turbines in an open flow, some wind tunnel results investigated the wake of turbine in one blade version [65]. Simulations performed in paper I gives very similar vortices traces as in Fig 11.



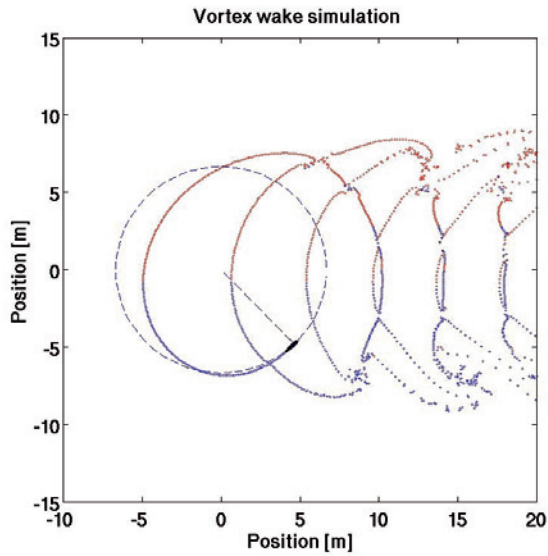


Figure 27. Vortex traces for the one blade version of [65] turbine

Usually in the wake studies, the line of vortices is allowed to break. This behavior is not accurate and is dependent on the core radius of the vortex model used. In order to make further investigation it is possible to refine the vortex lines as the wake expand and is distorted by Kelvin Helmholtz instabilities as in Fig 28.

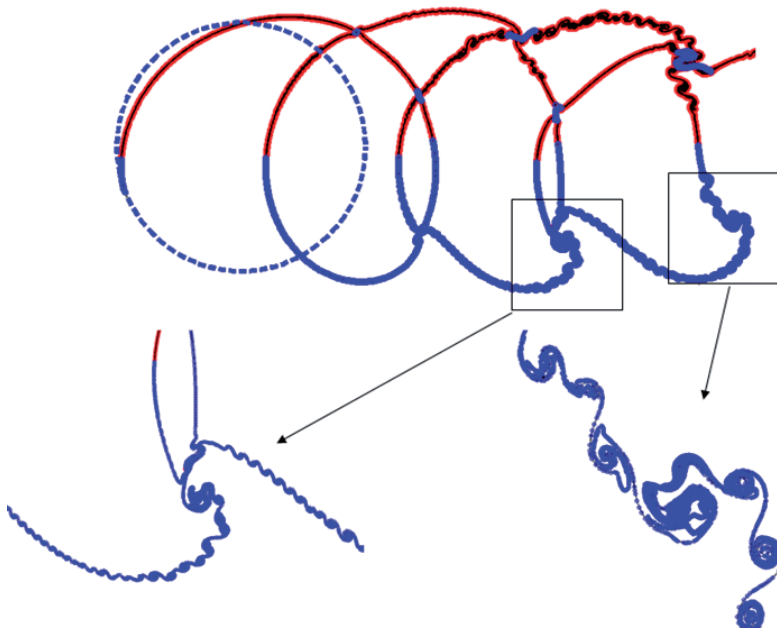


Figure 28. Wake of a single blade vertical axis H-rotor at low tip speed ratio with automatic vortex line refinement

#### 4.2.4. Aeroelastic analysis

Unfortunately very few reliable data is available to derive deflections of H-rotor blades in various operations. The standard mechanical model has been validated in the case of composite blades both against experiments and the standard FEM tool COMSOL Multiphysics [68].

The aeroelastic model Vore-ElasTechs developed in paper IV has been validated against Goland [69] analytical model on an assessment of the flutter speed.

The instability called flutter occurs when the aeroelastic coupling shifts the bending and twisting oscillation frequencies of a wing toward the same value. Aerodynamic forces are then responsible of a negative damping, which may increase the deformation and eventually break the wing.

Results between the aeroelastic model described in paper IV and the analytical results compare well knowing the different assumptions used to derive the analytical formulas (use of Theodorsen formulas [62]). A reduction has to be taken into account to include this assumption difference

Flutter Speed	Damped Oscillation	Stable Oscillation	Divergent Oscillation
Without Reduction Factor	117 m/s (261.7 mph)	118.5 m/s (265.1 mph)	120 m/s (268.4 mph)
With Reduction Factor $r=0.65$	151 m/s (337.8 mph)	152 m/s (340 mph)	153 m/s (342.3 mph)

Table 7. Evaluation of flutter speed with and without reduction factor (see Paper IV)

The Fig 29 reports the flap wise deflection and pitch angle history at the tip, for the three cases: damped, stable, and divergent motions. The harmonic oscillations appear clearly. The flutter speed predicted by VoreElasTechs is higher with the new reduction factor and compare in a conservative manner with the results of Goland [69] of a flutter speed at 175,7 m/s.

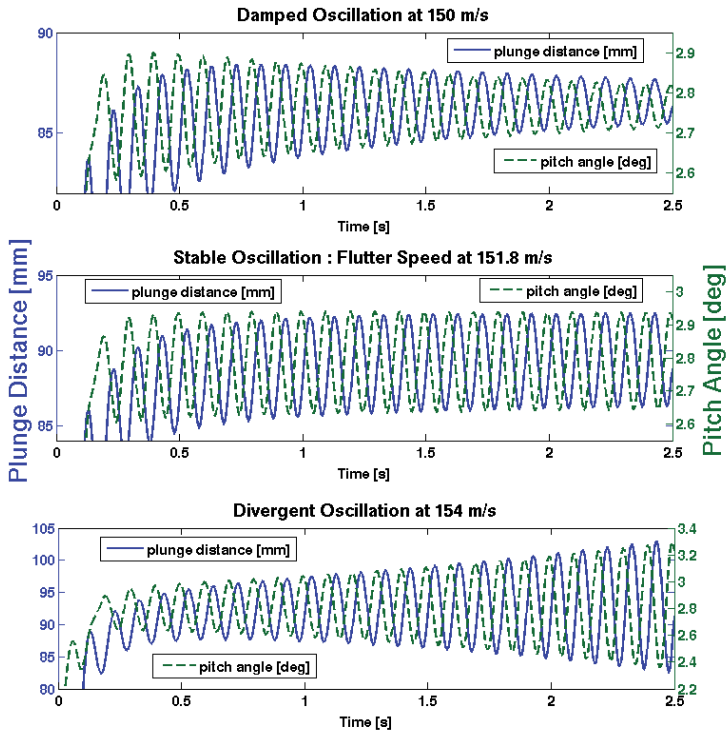


Figure 29. Pitch and Plunge history of Goland’s wing tip, close to flutter from Paper V

### 4.3 New design studies

Using the various tools developed in the present PhD thesis a wide number of turbines have been designed and load calculated. A summary of these design studies will be presented hereafter trying to emphasize the most important design parameters and their effects. To provide an overview of the main parameter influences, the following Table 9 shows where to focus first, leaving further parameters for fine tuning. The author is aware that the attached table is simplistic and cannot replace a true and precise optimization.

Design parameter	Main design influence	Secondary influence
Attachment point	Fatigue (downwind vs. upwind), Dynamic stall behaviour	Optimum TSR, Performance
Section pitch	Fatigue (downwind vs. upwind)	Optimum TSR, Performance
Section thickness	Dynamic stall behaviour	Performance
Section camber	None	Performance & Fatigue (downwind vs. upwind)
Overall section profile	Dynamic stall behaviour	Performance, Fatigue (downwind vs. upwind)
Chord to radius ratio	Links to attachment point and camber	
Solidity	Optimum TSR for optimum $C_p$ , Performance	
Blade Reynolds number	Performance	
Span plan form	Performance	
Number of blades	Vibrations, Solidity, Blade Reynolds number, Chord to radius	
Strut design	Performance, Fatigue (vibrations)	

Table 8. Simplified cross influence on VAWT aerodynamic design parameters

The design methodology depending on the design constraints can follow the steps used in M Whal MSc [6]

The following strategy is used in the design of the H-rotor turbine – this is a highly iterative process and therefore is placed here to help the reader.

1. Gather meteorological data and describe the wind resource on site.
2. Define the objective function and constraints (state the most important design criteria). The usual objective is to maximize the power output while reducing static and fatigue loads to decrease turbine costs. Standard constraints are a rated power at a certain wind speed, a maximum speed to be reached, frequencies to avoid together with wind climate definition using common standards parts...
3. List the parameters to consider in the design procedure. This is a mean of defining the level of detail in the analysis.
4. Fix some parameters to simplify and shorten the amount of time needed for the design process. Choose a square reference turbine (height and radius) to start the optimization with reference strut, etc... design parameters.
5. Based on the wind resource on site and performance data of earlier designs find a first tentative design fulfilling the power demand.
6. Refine the tentative design using a CMDMS and vortex design tool to ensure that all dimensions of the objective are achieved. One parameter at a time is optimized and then hold fixed in the following order. The parameters in the same line should be optimized together.
  - Rotor area
  - General strut design
  - Rotor solidity & optimum TSR & Number of blades
  - Blade thickness
  - Point of attachment & pitch angle
  - Blade camber
7. Verify the mean power output using the known wind regime and simulated aerodynamic performance together with load levels and coordinate with results from structures, generators and control systems

Each design loop from the aerodynamic side will produce

- A power curve
- The yielded number of MWh produced per year in the defined environment
- Extreme and fatigue loads on the wind environment defined
- The turbine Campbell diagram
- The basic control strategy
- Potential check
- Eventually a check of aeroelastic stabilities with the Eigen frequencies and Eigen modes of the blades, struts and rotor.

### 4.3.1 Marsta turbine

The main aerodynamic parameters for Marsta turbine are given in Table 7 in section 4.2. A picture of the built turbine can be found in Fig 30.



*Figure 30.* Marsta 12 kW turbine

From structural mechanical calculations it has been determined that a maximum blade tip speed of 40m/s is suitable, while a tip speed ratio around four is preferable in the variable speed range. Three blades are used in order to significantly smooth the load variations without deteriorating the overall performance as compared to two bladed turbines.

A chord of 0.25m was chosen, which gives a chord to radius ratio of 0.08, to ensure both a rather low optimal tip speed ratio while keeping the normal force coefficients due to flow curvature as low as possible. The Reynolds number will be acceptable, ranging from 0.3 millions at low wind speeds to 0.8 millions. The aspect ratio of 20 will limit the end tip losses to a

maximum of 16% of the overall power output. Concerning dynamic stall parameters the reduced frequency will be in the range of 0.02 at a tip speed ratio of 2.

Using the aforementioned method for these parameter ranges, the optimization process was limited to the symmetric NACA00XX series due to boundary layer uncertainties. The thick NACA0015 and NACA0018 were the best profiles delivering most of the power at the tip speed ratio of four. The NACA0018 was preferred to the NACA0015 because the peak power was obtained for a lower tip speed ratio while keeping the same power coefficient. The effect of placing the blades at the quarter chord point was also found to significantly increase the power extraction on the upwind part where the incoming flow is much cleaner than in the downwind part. The dynamic stall behaviour of the NACA0018 was also preferable in the low Reynolds number range considered. Variations in attachment position, inducing a small (few degrees) constant pitch, gave surprisingly different results. A particular care in the attachment procedure is highly recommended. The NACA0018 section has been extensively used both in previous Darrieus and H-rotor projects [70]. Its use is well documented in terms of vertical axis wind turbine motion [71], and it offers a good compromise in terms of thickness and dynamic behaviour.

The aerodynamic efficiency of this turbine finally reached 30% [66] (within 25% of the simulated one). The turbine was used extensively since 2007 to tune models and learn on simulation errors (for instance the strut influence was widely underestimated).

#### 4.3.2 A turbine for the South Pole Amundsen station

The IceCube project [6] is an international particle physics program which currently is building a neutrino telescope in connection to Amundsen Scott South Pole Station [72].

Today the Amundsen Scott station is powered by combustion engines. These consume large amounts of energy, especially if the fuel consumption caused by transportation to the South Pole is taken into account. This means not only pollution of atmosphere in Antarctica but also a very high cost of energy. Based on these two incentives, IceCube plans to be the first project introducing wind power at the Amundsen Scott station. The request from the IceCube project is to design a wind turbine producing between 26 and 43MWh per year. This result in mean power output of 3-5kW over the year at the root mean cube1 wind speed of 6.7 m/s at this site. The electrical power produced will be used to heat drilling equipment This project is a first step toward higher penetration of wind power in the existing electrical grid at the station.

The optimized results for the 5 kW turbine are grouped in the following table.

Dimensional parameters	
Wing section	NACA0018
Chord	45 cm
Number of blades	3
Turbine radius	5 m
Turbine height	10 m
Tip speed ratio (design)	4
Pitch (positive as out)	4°
Attachment point	Quarter chord
Rated wind speed	12 m/s
<b>Mean</b> power expected	5.2 kW
Strut section	NACA0025 (with flat back) 0.45cm length
Non dimensional parameters	
Solidity	0.27
Chord to radius ratio	0.09
Aspect ratio	22.2

Table 9. Main design parameters for the Ice Cube turbine (Paper VI)

The expected aerodynamic efficiency was expected to be around 38% at TSR 4.

#### 4.3.3 Other wind and underwater design studies

Other similar studies were performed for underwater turbines and higher power wind turbines. The data of the other wind turbine studies is confidential and will not be presented here. However it includes some preliminary studies for the EON Falkenberg vertical axis 200kW turbine and some final detailed studies for the ERICSSON Tower tube 20 kW 4 bladed turbine.

A concept study for an 8 bladed turbine for underwater applications has been performed in Paper V. Its wake is plotted in Fig 31. In this study the optimal tip speed ratio have to be reduced to avoid cavitations problems of the blades (TSR<3) in this application. The constraint of small height to avoid perturbing the boat traffic forces to use much more blades than usual.



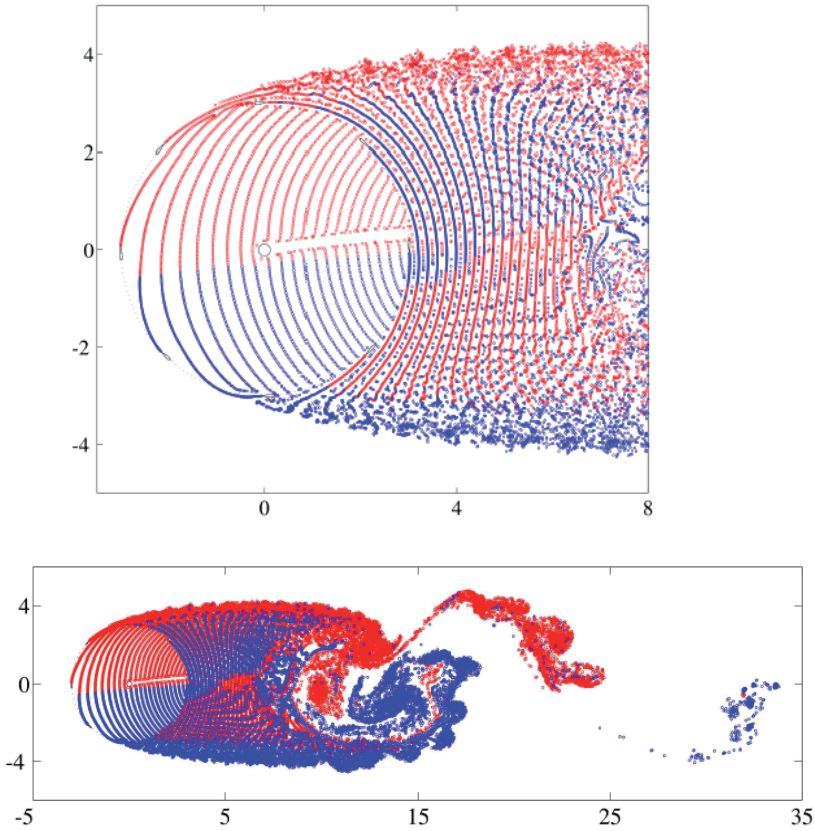


*Figure 31.* Concept study of the wake of an 8 bladed NACA0021 underwater turbine from Paper V

#### 4.3.4 Aeroelastic studies

Using the mechanical model validated and developed for the aeroelastic coupling in paper IV, it was possible to contain in the same tool the aerodynamic model using or CMDMS or the vortex model and fast elastic calculations. This new integrated model is perfectly suited for design studies as all results are fast but accurate enough to determine the critical next steps that can be investigated further using more advanced tools.

The model inputs are the blade and strut geometry, material definition and standard operation data. The typical outputs are the power output per wind bin, unsteady loads, deflections and Eigen frequencies. A concept study made on the blade and struts of a 4 blade turbines give the following results in terms of Blade and strut Eigen frequencies and modes in Fig 32.

## Eigenmodes Deformed Shape

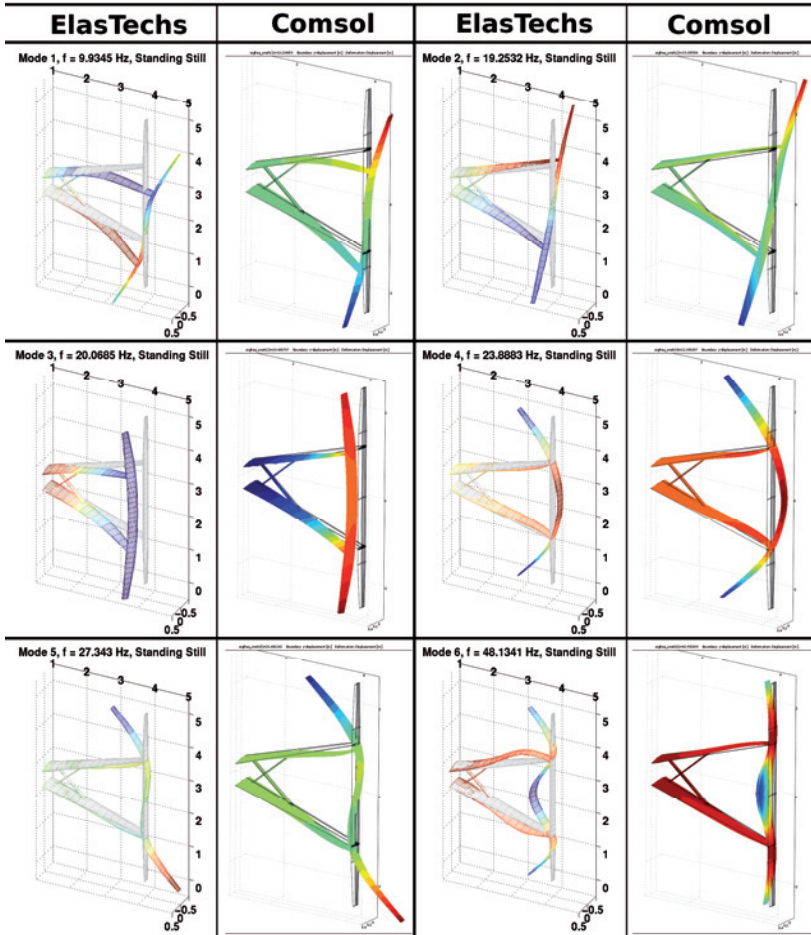


Figure 32. Comparison of Eigen modes and frequencies between COMSOL and VoreElasTechs

To conclude this paragraph we will compare the use of aeroelastic simulations compared to non coupled simulations for the very rigid Marsta blades. The resulting 2D-like flow is here modelled using the aerodynamic model of Paper II at different blade stations for a four bladed turbine (see Fig 33)

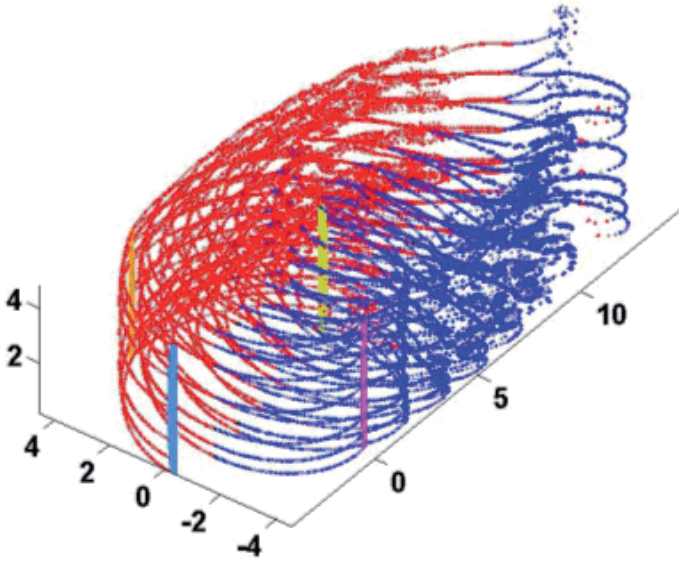


Figure 33. Wake results for 2D-like computation around a 4 bladed VAWT for aeroelastic computations.

The differences by using the retroactive loop between the fully coupled aeroelastic model and the one way coupled model are given in Fig 34 after a Fourier analysis of the tip displacement. The blades used for this concept study are very rigid. As a result all excitation frequencies appearing at the blade tip are clearly shown.

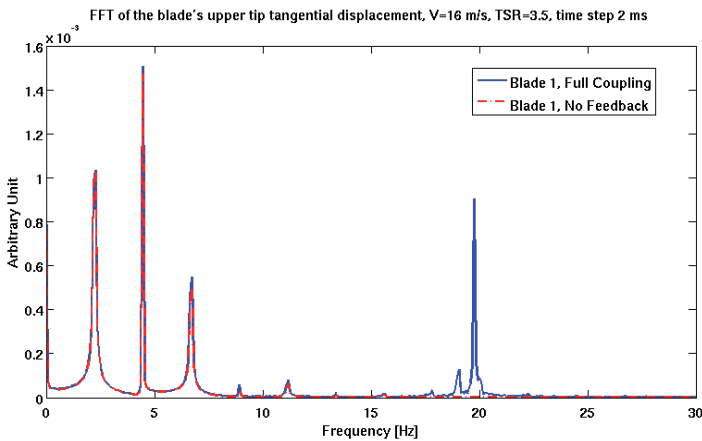


Figure 34. FFT of upper tip tangential displacement

## 4.4 Perspectives of the model

All methods herein developed have been done to model special parts of the flow and phenomenon useful to the VAWT designers. Although no model is able to capture all aspects of these complicated flows in a self contained one, all models have enough flexibility to design VAWT blades accurately and ensure good safety margins. The models developed herein are therefore fast to run (not more than several hours in the case of the full vortex advanced version of Paper II to several seconds per load cases for the basic result of Paper II) Moreover geometrical parameters such as airfoil section, attachment point, pitch angle, inflow angle and speed, can be both investigated in a static or dynamic way separately or commonly for each sections enhancing the optimization capabilities for VAWT blade designers.

The model developed in Paper II, consists in a more general unsteady simulation compared to Theodorsen [62], it can therefore be used in place of Theodorsen function to gather local unsteady 2D oscillations of wings in aeroelastic studies. This is valid for VAWTs but also a vast range of other flows such as airplane flows and others. A fast implementation of the Paper II model would be to study strut aeroelastic behavior by using an outer model giving an equivalent incoming flow at a 2D local section and using these parameters to study unsteady effects assuming the local macro flow will not change significantly.

Both for vertical and horizontal axis machines, one of the great challenge in wind farm optimization is the understanding, modelling and optimization of full wind farm. This leads to the assessment with various values of confidence level of the annual energy production which is the most important value for the farm developer,. These studies include wake modelling and turbine control optimization. Their aim is to extract as much power as possible while limiting loads on turbines and components in various wind directions following the farm implantation. Using Paper IV model, the time-averaged velocity wake deficit of a VAWT can be constructed as in Fig 35. The streamlines are really expanding as they hit the rotor circle. After 10 diameters, the wake degenerates into a vortex Karman street. These results are of course two dimensional and therefore are limited to high aspect ratio turbines.

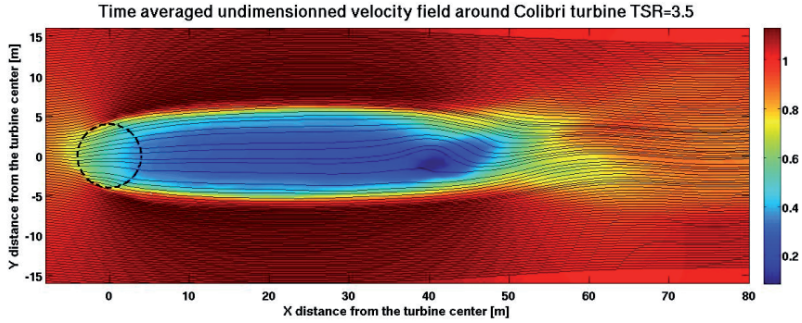


Figure 35. Time averaged velocity and streamlines around an H rotor at TSR=3.5.

The wake deficit can be calculated by evaluating the averaged velocity at fixed points in Fig 36.

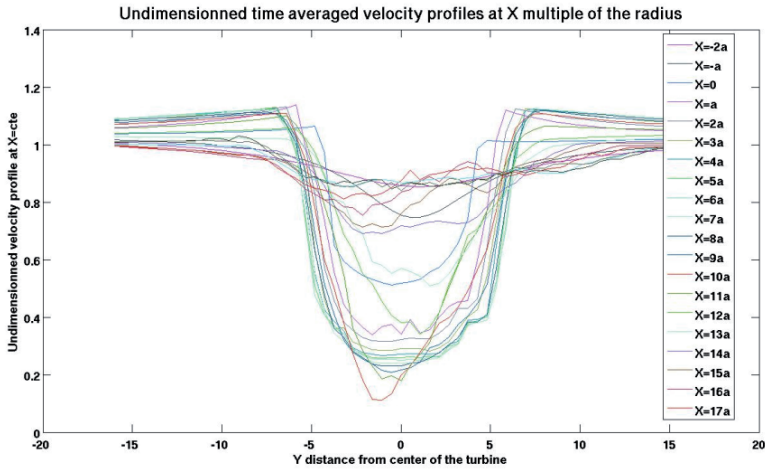
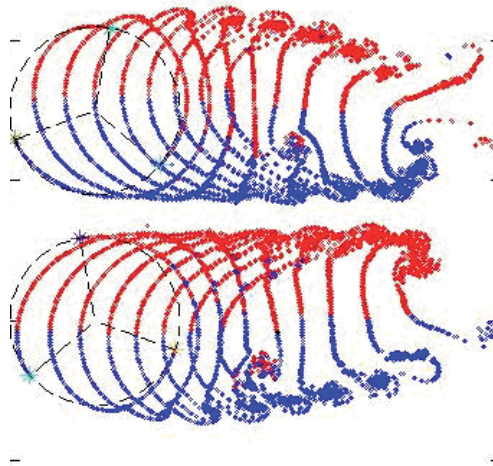


Figure 36. Time averaged velocity norm around an H rotor at TSR=3.5 at different locations perpendicular to the incoming wind speed.

Recent research performed by A Goude [73] showed that the rotating direction of the turbines inside the farm can be used to optimize the farm power output. The methods herein developed in Paper II, III and IV can assess as well the loads occurring on a turbine-to-turbine interaction to complete the optimization. An example of these abilities of the model showing the benefit of double counter rotating turbine arrangement can be seen in Fig 37.



*Figure 37.* Double VAWT arrangement of counter rotating turbines to enhance power performance from Paper IV

One interesting aspect included in the model of Paper II and IV is that using equivalent vortices incoming to the turbine and various flow direction angles to mimic turbulence and non homogeneous inflows, it is possible to study the effect on loads of turbulent inflows per section. Assuming that the flow slices do not interact with each other (which is clearly not strictly correct at certain Reynolds numbers), the Paper IV aeroelastic model can be generalized to 3D turbulent inflows with various wind mean directions.

Another interest of this semi analytical conformal mapping based model is the use of the exact solution (conformal mapping) rather than approximate solution (panel methods). Moving into full vortex methods aiming at solving full Navier Stokes equations, this is essential to have an accurate model of the main boundary, free of any disturbances. The use of conformal mapping also enhances the flow computation as it provides directly the better format for the flow evaluation at any distance from the section. However that use will be restricted to two dimensions. A computation analogous to what a DNS method would give can be found in Fig 38.

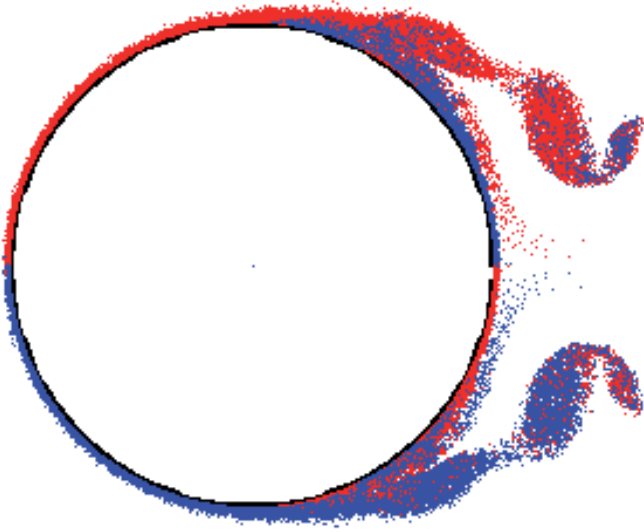


*Figure 38.* Traces of vortex flows around a starting cylinder at Reynolds number 9500 using the enhanced methodology of Paper II

# Suggestions for future work

The analytical theory developed in this thesis has highlighted specific flow phenomena that are believed to enhance our understanding of the flows around VAWT. However, the current PhD thesis analytical model using conformal mappings methods can not take into account important phenomena. These are, by decreasing order of importance:

- 3D effects (on wakes, dynamic stall and for tip vortices)
- 3D turbulent and inhomogeneous incoming flow
- Struts effects on the flow [74] and their aeroelastic behavior
- Dynamic detached flow at high angle of attacks and low tip speed ratios (the 2D vortex method which was tried in Paper II is limited to Reynolds numbers around 10 000)
- Viscous effects on foils and inside wakes (same remarks for limitations to Reynolds number around 10 000).

All these effects can be studied by using empirical double multiple streamtube models with corrections or by using 3D vortex methods based on vortex panels (including PSE schemes [75] to correctly account for viscosity effects) or specific CFD tools able to avoid the numerical diffusion in the shed vorticity.

For design studies, the double multiple streamtube methods will most probably be the best solution. However, the main limitations of these approaches are that they don't contain any unsteadiness and are therefore not suited as such for aeroelasticity calculations.

From the 2D model, it is possible to adapt the current model into the low TSR region by using double vortex sheets models triggered by a semi empirical model for the position of the separation point. Several attempts using double sheets reduced to discrete points did not lead to significant results. However 3D vortex sheet models have been tried [76] and should lead to better results. On the numerical part, ad hoc methods for fast summations of 3D singularities should also be developed.



# Summary of papers

All the work presented here is based on the same concept, an H-rotor. The papers can be divided into two parts, the first part deals with the theory used to develop the aerodynamic simulation toolbox. The second part is more focused on the use of the tools to design turbines and compare the results of the simulations with H-rotor measurements.

Paper I defines an algorithm to transform complex sections into a set of circles. Paper II is using the geometrical simplification of Paper I to get exact analytical solutions of H-rotor aerodynamic sections. Paper III provides the semi analytical generalization of Paper III into multiple blade H-rotor sections. Paper IV uses the results of Paper II to couple the aerodynamics with structural mechanics to investigate aeroelastic behavior of VAWTs. Paper V beneficiaries from the toolbox defined to design an underwater turbine. Paper VI highlights the design of the 12kW Marsta machine. Paper VII and Paper VIII are collecting the first results from the Marsta turbine and explain deviations with simulations. The author's contribution to each paper is given below.

## ***Paper I. Conformal mapping and efficient boundary element method without boundary elements for fast vortex particle simulations***

This paper is a research paper giving an algorithm to perform fast conformal mapping of  $N$  airfoil sections into a circle. This paper also enhance why the use of conformal mapping technique is interesting to study complex vortex flows. This paper prepares the work achieved in paper II.

The author has done all biographical reviews, equation finding and algorithm coding in Matlab. The equations and results were checked and reviewed by the coauthors. The author has written the whole paper.

Published in European Journal of Mechanics – B Fluids

## ***Paper II. Analytical solutions for a single blade in vertical axis turbine motion in two-dimensions***

This is a research paper giving exact solutions and an algorithm to compute fast the unsteady aerodynamics of airfoil sections.

The author has done all biographical reviews, derived the equations and made the code except the fast multipole program which was made by the coauthors. The author has written the paper except the paragraph treating about the Fast Multipole Method code which was written by the coauthors.

Published in European Journal of Mechanics– B Fluids

***Paper III. A Multi-Body Vortex Method Applied to Vertical Axis Wind Turbines.***

This is a research paper giving iterative solutions of H-rotor flows in two dimensions. The iterative solution can be found up to any desired level of accuracy.

The author has provided the conformal mapping program and guidelines for the algorithm development, he has checked, reviewed and corrected all equations and have provided ways to improve the algorithms as the supervisor of the main author. The writing of the paper was made in common with other co-authors.

Submitted to the European Journal of Mechanics

***Paper IV. Fast aeroelastic model for straight bladed vertical axis wind and hydro turbines***

This is a research paper giving the coupling between the aerodynamic model of paper II with adaptation and the structural model. The author has developed the coupling between the two models into a complete program. The author wrote the bibliography review and the aerodynamic part. The result analysis and the rest of the paper were written in cooperation with the co-authors.

Submitted to the Wind Engineering Journal

***Paper V. Matching a permanent magnet synchronous generator to a fixed pitch vertical axis turbine for marine current energy conversion***

This paper is a research paper showing the design and construction of a generator suited for vertical axis under water turbines. The author has calculated the three VAWT designs used and has performed preliminary wake studies for design cases. The paper was written in cooperation with the coauthors.

Published in. IEEE Journal of Ocean Engineering, vol 34, no1, pp24-31, Jan 2009.

***Paper VI. Design of a 12kW vertical axis wind turbine equipped with a direct driven PM synchronous generator***

This paper describes the design of a complete 12 kW VAWT, from generator to blades. The electric design as well as aerodynamic and structural design has been performed using different simulation methods. For the blade design and loads, the simulation tool was derived and programmed by the author. The author has taken a major part in designing the blades. The author has written part of the paper.

Presented with a poster at the European Wind energy Conference & Exhibition 2006.

***Paper VII. Experimental results from a 12 kW vertical axis wind turbine with a direct driven PM synchronous generator***

This paper presents the construction of the generator and the complete 12 kW VAWT. It also presents the site where the turbine is situated, which has a well characterized wind climate. The data treatment method is explained. Experimental data on rotational speed and electrical power is presented. Furthermore, a preliminary CP-TSR curve is presented with data from measurements on a day with high turbulence. This first experimental data is as expected considering the highly turbulent wind conditions. The author has taken part in design and construction of the wind turbine. The author has taken part in experiments and data treatment. The author has written part of the paper.

Presented with a poster at the European Wind energy Conference & Exhibition 2007.

***Paper VIII. Progress of control system and measurement techniques for a 12 kW vertical axis wind turbine.***

This paper presents parts of the electrical system of the 12 kW VAWT. The first part is the voltage control load that keeps the rotational speed constant. The rotational speed is adjusted manually and can be adapted to the prevailing wind conditions. The second part of the electrical system is the electrical starter, which accelerates the turbine until it is rotated by the wind. The paper includes experimental results showing control of the rotational speed, both during operation and during start-up. Furthermore, the paper presents the measurement system that is under development. The author has taken part in design and construction of the wind turbine. The author has taken part in experiments and data treatment. The author has written part of the paper.

Presented orally by J. Kjellin at the European Wind energy Conference & Exhibition 2008. Published in proceedings. Reviewed conference paper.

# Conclusion

The blades are governing the turbine's efficiency and their power output is primarily given by their design. The blades and rotor structure should be light and not over dimensioned to ensure competitiveness of the whole machine.

The challenges in vertical axis wind turbines have not yet been all mastered. Past experiences showed that good rotor design has not reached a matured and reliable state of the art.

The following thesis reviews the pioneer projects to grow up the vertical axis wind turbine technology. Then the underlining aerodynamic specificities of the vertical axis turbines have been explained. The aerodynamic simulation tools that have been used by past blade and rotor designers are reviewed. It has been found that a reasonably fast (regarding computer power) and accurate (regarding comparison with experimental results) was still lacking in the field.

The object of the current PhD thesis was to apply and generalize the 1900's analytical theory developed by NACA and NASA for first aircraft wings' development, then widely used to derive physical airfoil characteristics by hand calculation getting back to the well known circle analysis. It shows that this theory can be widely generalized to airfoils with complex shapes in complex motions placed in complex vortex flows, conditions ideally apply to vertical axis wind turbines.

Using modern computing methods in conjunction with the old analytical developments, it is shown that new simulation tools can be implemented successfully. This leads to an important step forward in the understanding of flow features in the field of unsteady aerodynamics and especially vertical axis wind turbines aerodynamics. However the theory is restrained to two dimensional calculations and is therefore restrained.

Finally by using locally two dimensional results, the fluid – structure interaction has been implemented to study aeroelastic behavior of vertical axis turbines with long straight blades.

A double multiple streamtube model has also been developed to complete the aerodynamic and aeroelastic toolbox described. All models have been applied in various H-rotor designs under operations and development at Uppsala University.

# Acknowledgments

First of all I would like to thank my two supervisors for this PhD thesis: Olov Agren and Hans Bernhoff. Olov was always open for passionate discussions (although cold during winters) on conformal mapping or mathematical aspects and significantly contributed to the theory described here. Hans was always looking to engineering applications and design which was really a good fit to reorient this PhD thesis when it was turning to be too abstract and theoretical.

I would like to kindly thank Mats Leijon which offered me this really great PhD subject and the opportunity to perform all this work.

I would like to warmly thank the other key players without which my PhD would have not been so fun: Mathias Bouquerel, David Österberg Mats Wahl and of course Stefan Engblom. You helped me to explore new interesting paths and way forward. I really liked our interactions together.

Thirdly I would like to thank all my colleagues in the department of Electricity which were so much devoted like me towards wind and hydro power: manythanks to Sandra, Jon, Fredrik, Andreas, Marcus, Anders, Thomas, Katarina, Karin, Marten I really enjoyed the talks and discussion about Swedish habits and culture as well as your open minds..

I would also like to thank the whole staff of the Centre for renewable energy conversion and the university staff which always provides very precious advices and valuable help.

Finally I would like to thank all my closest friends and family during this fruitful time in Sweden and I deeply apologize for having been so focused on these abstract concepts that I could not talk about anything else...

# Summary in Swedish

## Analytiska aerodynamiska simuleringsverktyg för vertikalaxlade vindkraftverk

Vindkraften är det idag snabbast växande förnybara energislaget och kan bidra till att minska de totala CO<sub>2</sub>-utsläppen från elproduktion. Den horisontalaxlade, trebladiga propellern har dominerat den storskaliga teknikutvecklingen i mer än två decennier och det horisontalaxlade konceptet är idag helt dominerande på marknaden. Denna avhandling berör en alternativ typ av vindkraftverk med raka blad som roterar kring sin vertikala axel, kallad 'VAVT' från VertikalAxlad VindTurbin eller 'H-rotor' då den på håll ser ut som ett 'H'. En kort översikt över de viktigaste skillnaderna mellan de horisontal- och vertikalaxlade koncepten har presenterats. Fokus för avhandlingen är aerodynamik för vindturbinens vingar.

### **H-rotorkonceptet**

I denna avhandling studeras en VAVT av H-rotortyp, d.v.s. med raka blad som stöds av två bärramar. H-rotorn är omnidirektionell och med raka blad kan en enkel bladprofil användas. Axelns orientering gör att generatoren kan placeras på marken och den är därmed direkt driven, d.v.s. ingen växellåda behövs. Konceptet möjliggör en lättare tornkonstruktion. H-rotorn har en lägre optimal vingspets hastighet vilket begränsar buller. Kraftverket har elektriskt kontrollerad passiv stallreglering vilket eliminerar bladvridning, d.v.s. bladen är fasta.

### **Metod**

Det första steget för att åstadkomma aerodynamiskt effektiva turbiner är att designa effektiva blad. Det krävs en god förståelse av de fysikaliska fenomenen samt effektiva simuleringsverktyg för att modellera bladen. Teorin för aerodynamiken för flödet genom en rakbladig vertikalaxlad turbin presenteras tillsammans med standardiserade aerodynamiska simuleringsverktyg för rotordesign. Simuleringsverktygen har även tidigare använts för att designa bladen. En godtagbart snabb (beräkningseffektiv) och korrekt modell (jämfört med experimentella resultat) har tidigare saknats inom detta område.

Analytiska metoder kan användas för att modellera komplexa flöden för enkla geometrier. En konform avbildningsmetod, som transformerar en godtycklig uppsättning av sektioner till en enkel uppsättning av geometriska cirklar, har utvecklats för att underlätta beräkningen. Analysen har generaliserats för att simulera flera rörliga sektioner i komplexa flöden och krafter och vridmoment på bladen beräknas. Dessutom har den snabba semianalytiska, aerodynamiska algoritmen accelererats genom att en effektiv flerpolygon metod har utvecklats. Metoden har implementerats för att kunna hantera ett stort antal virvlar i luftflödet tillsammans med en enkel strukturell modell av rotern. Detta gör det möjligt att undersöka aeroelastiska instabiliteter och förstå hur dessa kan minimeras med lämplig design.

Tillsammans med dessa avancerade simuleringsverktyg har en standard dubbel multipel strömrörmodell utvecklats och använts för att utforma flera vertikalexlade turbiner från 2 kW till 20 kW.

### **Perspektiv**

Alla här utvecklade metoder berör fenomen användbara för VAVT-designers. Även om ingen modell kan fånga alla aspekter av dessa komplicerade flöden har de presenterade modellerna tillräckligt med flexibilitet för att utforma VAVT-blad. De här utvecklade modellerna är snabba: mellan några timmars processortid för den fullständiga virvelversionen (se Papper II) ned till några sekunder per lastfall. Dessutom kan geometriska parametrar (såsom fastsättningspunkt, pitchvinkel, inflödesvinkel) undersökas både i en statisk och en dynamisk modell var för sig eller gemensamt för varje sektion.

Både för vertikal- och horisontalexlade maskiner är optimering av hela vindkraftparken en stor utmaning: att bedöma den totala årliga energiproduktionen är det viktigaste för parkutvecklare. Dessa studier inkluderar vakmodeller och optimering av turbinstyrningen. Målet är att få ut så mycket effekt som möjligt och samtidigt begränsa belastningen på turbiner och komponenter i olika vindriktningar.

### **Slutsats**

Det vertikalexlade vindkraftverkets blad styr turbinens effektivitet. Bladens effektivitet ges i första hand av dess utformning. Bladen och hela rotorstrukturen bör vara lätt, inte överdimensionerade, för att säkerställa konkurrenskraften för hela vindkraftverket. Denna avhandling berör ett nyckelområde inom framväxten av en kommersiellt konkurrenskraftig vertikalexlad vindkraftteknik. De aerodynamiska simuleringsverktyg som har använts av tidigare blad- och rotordesigners saknar önskvärd snabbhet och precision. Syftet med den aktuella avhandlingen är att tillämpa och generalisera 1900-talets analytiska teori. Den utvecklades av NACA och NASA för de första flygplansvingarna. Denna teori har generaliserats till allmänna vingsektioner i komplexa rörelser och virvelflöden, d.v.s. vilkor

som är ideala för att simulera vertikala vindkraftverk. De nya simuleringsverktygen har kunnat implementeras framgångsrikt med hjälp av moderna IT verktyg. Detta har lett till ett viktigt steg framåt i förståelsen av vertikala vindkraftverks aerodynamik. Men teorin är begränsad till tvådimensionella beräkningar.

Slutligen, genom att använda lokalt tvådimensionella flödesmekaniska modeller med strukturinteraktion har aeroelastiskt beteende hos vertikalaxlade vindkraftverk med långa raka blad kunnat studeras. En dubbel strömtubsmodell har också utvecklats för att komplettera den aerodynamiska och aeroelastiska verktygslådan. Alla modeller har tillämpats i olika H-rotordesigner i linje med verksamheten och utvecklingen vid Uppsala universitet.



# References

1. B. Barré, Tout sur l'énergie nucléaire : d'atome à Zirconium , AREVA Editions, 2003.
2. LULUCF: Land Use, Land Use Change and Forestry, IPCC 2007
3. HIS Emerging Energy Research, Europe Wind Plant Ownership Rankings: Top 10 Markets, Year-End 2009
4. J. Acher. China became top wind power market in 2009 *Reuters*, 29 March 2010. Retrieved: 8 August 2010.
5. O. Ågren, M. Berg, and M. Leijon. A time-dependent potential flow theory for the aerodynamics of vertical axis wind turbines. *J. Appl. Phys.*, 97:104913, 2005.
6. M. Wahl, MSc thesis, Designing an H-rotor type Wind Turbine for Operation on Amundsen-Scott South Pole Station, Uppsala, December 7, 2007
7. D. Osterberg, MSc thesis, Aerodynamics of Vertical Axis Wind Turbines, Multi-Body Unsteady Aerodynamics in 2D using a Vortex Method, Uppsala, November 16, 2007
8. M. Bouquerel, Modèle aéroélastique pour éolienne à axe vertical, ENPC rapport de stage long, July 2008
9. A. Solum and M. Leijon. Investigating the overload capacity of a direct driven synchronous permanent magnet wind turbine generator designed using high-voltage cable technology. *International Journal of Energy Research*, 31(11):1076 – 1086, 2007.
10. A. Solum. Permanent magnet generator for direct drive wind turbines. UURIE 303-06L, ISSN 0349-8352, Division for Electricity, Box 534, 75121 Uppsala, Sweden, 2006. Licentiate Thesis.
11. S. Eriksson, H. Bernhoff and M. Leijon. Evaluation of different turbine concepts for wind power. *Renewable and Sustainable Energy Reviews*, 12(5):1419-1434, 2008.
12. S. Eriksson and H. Bernhoff. Generator-damped torsional vibrations of a vertical axis wind turbine. *Wind Engineering*, 29(5): 449-462, 2005.
13. S. Eriksson, A. Solum, M. Leijon and H. Bernhoff. Simulations and experiments on a 12 kW direct driven PM synchronous generator for wind power. *Renewable Energy*, 33(4):674-681, 2008
14. S. Eriksson, H. Bernhoff and M. Leijon. FEM simulations and experiments of different loading conditions for a 12 kW direct driven PM synchronous generator for wind power. Conditionally accepted for publication in *International Journal of Emerging Electric Power Systems*
15. A. Iida, A. Mizuno, and K. Fukudome. Numerical simulation of aerodynamic noise radiated from vertical axis wind turbines. Kyoto, Japan, 2004. Proc. Of ICA 2004, The 18th International Congress on Acoustics, 2004
16. T. Ackermann and L. Söder. An overview of wind energy-status 2002. *Renewable and Sustainable Energy Reviews*, 6(1 – 2):67 – 127, 2002.

17. G.M. Joselin Herbert, S. Iniyan, E. Sreevalsan, and S. Rajapandian. A review of wind energy technologies. *Renewable and Sustainable Energy Reviews*, 11(6):1117 – 1145, 2007.
18. Shikha, T.S. Bhatti, and D.P. Kothari. Early development of modern vertical and horizontal axis wind turbines: A review. *Wind Engineering*, 29(3):287 – 299, 2005.
19. S.J. Savonius. Rotor adapted to be driven by wind or flowing water. US Patent No. 1.697.574, 1929.
20. R.W. Righter, *Wind Energy in America: A History*, University of Oklahoma Press, p. page44, ISBN 0806128127, 1996
21. J.F. Manwell, J.G. McGowan, and A.L. Rogers. *Wind energy explained*. John Wiley and Sons Ltd., Amherst, USA, 1st edition, 2002.
22. B. Jürgens, W Fork. *Faszination Voith-Schneider-Propeller, Geschichte und Technik. The Fascination of Voith-Schneider Propellers, History and Engineering*, Hamburg 2002.
23. B. Jürgens, HJ Heinke. Voith Schneider Propeller (VSP) - Investigations of the cavitation behaviour. First International Symposium on Marine Propulsors, SMP'09, Trondheim, Norway, June 2009
24. IP2H AG, Aircraft, European Patent, EP1685024 B1
25. ECONCERN, E.A. Rossen, P.C. Scheijgrond, Device for the utilization of wave energy, Patent WO2002044558A1.
26. Ponte Di Archimede SPA, D. Coiro, E.M.A. Maticena, A. Moroso, N Fabrizio, F Nicolosi, Vertical axis water current turbine Patent WO2005024226 A1
27. JM Darrieus, patent, BE336740A
28. C.M. Fry, H. Hise, Wind driven, high altitude power apparatus, Patent US4084102 A
29. Global Energy Co Ltd, Wind power generator, windmill, and spindle and blade of the windmill, Patent US7040858 B2
30. J. Moser, Wind-powered rotor, Patent US5269647 A,
31. GCK Technology Inc, M. Gavasheli, Turbine for free flowing water, Patent WO2001048374 A2
32. J. Katz, A. Plotkin. *Low speed aerodynamics, from wing theory to panel methods*; Mac-Graw Hill: 1991.
33. B.G. Newman, Actuator-disk theory for vertical axis wind turbines. *J. Wind Eng. And Industrial Aerodynamics*, 15/3, 1983, p.347-355.
34. J. W. Oler, J. H. Strickland, B. J. Im, and G. H. Graham. Dynamic stall regulation of the darrieus turbine. Sandia National Laboratories, 1983.
35. J. H. Strickland, B. T. Webster, and T. Nguyen. A vortex model of the Darrieus turbine: an analytical and experimental study. *Transactions of the ASME*, 1979.
36. B. G. Newman. Multiple actuator-disc theory for wind turbines. *Journal of Wind Engineering and Industrial Aerodynamics*, 1986.
37. O. Holme. A contribution to the aerodynamic theory of the vertical-axis wind turbine. In *International Symposium on Wind Energy Systems - Cambridge, England*, 1976.
38. J. B. Fanucci and R. E.Walters. Inovative wind machines: the theoretical performance of a vertical axis wind turbine. In *Vertical-Axis Wind Turbine Technology Workshop Sandia Laboratory SAND765586*, 1976.
39. I. Paraschivoiu. *Wind turbine design: with emphasis on Darrieus concept*. Polytechnic International, Press, Montreal, 2002.
40. G.F. Homicz. Numerical Simulation of VAWT Stochastic Aerodynamic Loads Prodiced by Atmospherice Turbulence : VAWT-SAL Code. Sandia Laboratories, SAND91-1124, Albuquerque, NM, septembre 1991.

41. R. J. Templin. Aerodynamic performance theory for the nrc vertical-axis wind turbine. National Research Council of Canada, LTR-160, 1974.
42. C. S. Ferreira, H. Bijl, G. van Bussel, and G. van Kuik. Simulating dynamic stall in a 2d vawt: modeling strategy, verification and validation with particle image velocimetry data. In 45th AIAA Aerospace Sciences Meeting and Exhibit ,AIAA 2007-1366, 2007.
43. C. S. Ferreira, G. van Bussel, F. Scarano, and G. van Kuik. 2d piv visualization of dynamic stall on a vertical axis wind turbine. In 45th AIAA Aerospace Sciences Meeting and Exhibit ,AIAA 2007-1366, 2007.
44. A. Lida, K. Kato, and A. Mizuno. Numerical simulation of unsteady flow and aerodynamic performance
45. E. B. Saff & A. D. Snider, 2003, *Fundamentals of Complex Analysis with Applications to Engineering and Science*. Third edition, 2003. ISBN 0-13-907874-6.
46. T. Theodorsen. Theory of wing sections of arbitrary shape. Rept NACA, 411, 1931.
47. G. Couchet. *Mouvement plan d un fluide en presence d'un profil mobile*. Gauthier Villars, 1956.
48. J.J. Bertin, M.L. Smith *Aerodynamics for engineers*. Prentice hall, 1989
49. S. G. Krantz, 1999. In *Handbook of Complex Variables*. 86-87, MA: Birkhäuser, Boston.
50. D. Gaier, 1964. *Konstruktive Methoden der konformen Abbildung*. Berlin, Springer.
51. F. L. Ponta, P. M. Jacovkis, September 2001, A vortex model for Darrieus turbine using finite element techniques, *Renewable Energy*, Volume 24, Issue 1 , Pages 1-18.
52. K. Streitlien, M. S. Triantafyllou, 1995, Force and Moment on a Joukowski Profile in the. Presence of Point Vortices. *AIAA JOURNAL*. Vol. 33, No. 4, April 1995
53. R.R. Clements, 1973, An inviscid model of two dimensional vortex shedding, *Journal of Fluid Mechanics* 57 (2) (1973) 321–336.
54. L.M.. Milne-Thomson. *Theoretical aerodynamics*. 4th edition; Dover Publications Inc: New York, 1973.
55. R.E. Wilson, P.B.S. Lissaman, M. James, W.R. McKie. Aerodynamics loads on a Darrieus rotor blade. *Journal of Fluids Engineering* March 1983; 105(53).
56. H.B. Squire, A.D. Young. The calculation of the profile drag of aerofoils, R&M No 1838, A:R:C. Technical report, London 1938.
57. H. Schlichting, K. Gersten. *Boundary layer theory*; Springer-Verlag: Berlin Heidelberg, 2000.
58. P.G. Migliore, W.P. Wolfe, J.B. Fanucci. Flow curvature effects on Darrieus turbine blade aerodynamics. *Journal of Energy* 1980; 4(2).
59. D.J. Sharpe. Refinements and developments of the multiple streamtube theory for the aerodynamic performance of vertical axis wind turbines. *Wind Energy Conference*. Cranfield, 1984.
60. A. Suddhoo, I.M. Hall. 1985. Test cases for the plane potential flow past multi-element aerofoils. *Aeronautical Journal*, 89:403—414
61. R.A. Piziali, Sep 1994, 2-D and 3-D Oscillating wing aerodynamic for a range of angles of attack including stall, NASA TM 4632, Technical report 94-A-011.
62. T. Theodorsen. General theory of aerodynamic instability and the mechanism of flutter, NACA-ARR-1935, NACA-TR-496.
63. J. Moran. *An Introduction to Theoretical and Computational Aerodynamics*, Wiley, New York 1984.

64. L.B. Wang, L. Zhang, N.D. Zeng, A potential flow 2D vortex panel model, Applications to vertical axis straight blade tidal turbine, *Energy Conversion and Management* 48 (2) (February 2007) 454–461.
65. P.C. Klimas, Darrieus rotor aerodynamics. *Trans. ASME J. Solar Energy Engng.* 104 (1982), pp. 102–105, 1982
66. J Kjellin, F Bulow, S Eriksson, A Goude., P Deglaire, M Leijon, H Bernhoff, Power Coefficient Measurement on a 12 kW Straight Bladed Vertical Axis Wind Turbine, submitted to ...
67. R. E. Gormont, A mathematical model of unsteady aerodynamics and radial flow for application to helicopter rotors, *Tech. Rep., USAAV Labs., tR 72-67*, 1973.
68. G. Dahlquist, 33 years of numerical instability: Part 1, *BIT*, 35:1 (1985), 188–204.
69. M. Goland. The flutter of a uniform cantilever wing. *Journal of applied mechanics*, Vol. 12, No. 4, December 1945, pp. 198-208.
70. I.D. Mays, C.A. Morgan. The 500KW VAWT Demonstration project. EWEC 1989.
71. R.K. Angell, P.J. Musgrove, RAMcD Galbraith. Collected data for tests on a NACA0018 airfoil. G.U. Aero Report 8817, 1988; 3.
72. L. Simion et P. Henarejos, « ICE CUBE, un télescope taillé dans la glace », *Ciel & Espace*, juin 2006.
73. A. Goude, O. Agren, Numerical simulation of a farm of Vertical Axis marine current turbines. *Proceedings of the ASME 2010 29th International Conference on Ocean, Offshore and Arctic Engineering OMAE2010*, June 6 - 11, 2010, Shanghai, China
74. A. Goude, S. Lundin, M. Leijon, A parameter study of the influence of struts on the performance of a vertical-axis marine current turbine, in: *Proceedings of the 8th European Wave and Tidal Energy Conference*, Uppsala, Sweden, 2009.
75. S. Subramaniam, 1996, A new mesh-free vortex method, PhD thesis Florida state University, 1996.
76. C. Ferreira, K. Dixon, C. Hofemann, G. van Kuik, G. van Bussel, The VAWT in Skew: Stereo-PIV and Vortex Modeling, presented at the 47th AIAA Aerospace Sciences Meeting, 5 - 8 January 2009, Orlando, Florida



# Acta Universitatis Upsaliensis

*Digital Comprehensive Summaries of Uppsala Dissertations  
from the Faculty of Science and Technology 774*

Editor: The Dean of the Faculty of Science and Technology

A doctoral dissertation from the Faculty of Science and Technology, Uppsala University, is usually a summary of a number of papers. A few copies of the complete dissertation are kept at major Swedish research libraries, while the summary alone is distributed internationally through the series Digital Comprehensive Summaries of Uppsala Dissertations from the Faculty of Science and Technology. (Prior to January, 2005, the series was published under the title “Comprehensive Summaries of Uppsala Dissertations from the Faculty of Science and Technology”.)

Distribution: [publications.uu.se](http://publications.uu.se)  
urn:nbn:se:uu:diva-132073



ACTA  
UNIVERSITATIS  
UPSALIENSIS  
UPPSALA  
2010